JAMES | Journal of Advances in Modeling Earth Systems

RESEARCH ARTICLE
10.1029/2019MS001688

Special Section:
The UK Earth System Models for CMIP6

Strong Dependence of Atmospheric Feedbacks on Mixed-Phase Microphysics and Aerosol-Cloud Interactions in HadGEM3

A. Bodas-Salcedo[1], J. P. Mulcahy[1], T. Andrews[1], K. D. Williams[1], M. A. Ringer[1], P. R. Field[1], and G. S. Elsaesser[2]

[1]Met Office Hadley Centre, Exeter, UK, [2]Goddard Institute for Space Studies, Columbia University/NASA, New York, NY, USA

Key Points:
- Large changes in shortwave cloud feedbacks exist between two recent configurations of Met Office model
- Changes in midlatitude feedbacks explain most of the global-mean differences
- The new aerosol and mixed-phase schemes explain most of the feedback differences

Correspondence to:
A. Bodas-Salcedo,
alejandro.bodas@metoffice.gov.uk

Citation:
Bodas-Salcedo, A., Mulcahy, J. P., Andrews, T., Williams, K. D., Ringer, M. A., Field, P. R., & Elsaesser, G. S. (2019). Strong dependence of atmospheric feedbacks on mixed-phase microphysics and aerosol-cloud interactions in HadGEM3. *Journal of Advances in Modeling Earth Systems*, *11*. https://doi.org/10.1029/2019MS001688

Received 18 MAR 2019
Accepted 9 MAY 2019
Accepted article online 16 MAY 2019

Abstract We analyze the atmospheric processes that explain the large changes in radiative feedbacks between the two latest climate configurations of the Hadley Centre Global Environmental model. We use a large set of atmosphere-only climate change simulations (*amip* and *amip-p4K*) to separate the contributions to the differences in feedback parameter from all the atmospheric model developments between the two latest model configurations. We show that the differences are mostly driven by changes in the shortwave cloud radiative feedback in the midlatitudes, mainly over the Southern Ocean. Two new schemes explain most of the differences: the introduction of a new aerosol scheme and the development of a new mixed-phase cloud scheme. Both schemes reduce the strength of the preexisting shortwave negative cloud feedback in the midlatitudes. The new aerosol scheme dampens a strong aerosol-cloud interaction, and it also suppresses a negative clear-sky shortwave feedback. The mixed-phase scheme increases the amount of cloud liquid water path (LWP) in the present day and reduces the increase in LWP with warming. Both changes contribute to reducing the negative radiative feedback of the increase of LWP in the warmer climate. The mixed-phase scheme also enhances a strong, preexisting, positive cloud fraction feedback. We assess the realism of the changes by comparing present-day simulations against observations and discuss avenues that could help constrain the relevant processes.

1. Introduction

The Hadley Centre climate model is used for both understanding climate processes and climate change and to provide projections of future climate on seasonal to centennial timescales. Understanding the nature and magnitude of the atmospheric feedbacks operating in the model is central to these applications. The feedbacks also determine widely used metrics such as equilibrium climate sensitivity (ECS), which are often used to characterize a model's global response to radiative forcing.

Once the configuration of a new model has been finalized, it is therefore important to examine the feedbacks relative to its predecessor and to try and identify how changes made to the representation of physical processes may have influenced their evolution. This is especially true for cloud radiative effects as there is often no consensus on the representation of many cloud processes in models (e.g., aerosol-cloud interactions). This inevitably leads to a large spread in the cloud responses to warming, which in turn contributes to similarly large spread in the climate sensitivity (e.g., Andrews et al., 2012).

Here we examine the atmospheric feedbacks in the latest climate configuration of the Hadley Centre Global Environmental model (HadGEM3-GC3.1; Williams et al., 2018), relative to our previous climate configuration (HadGEM3-GC2; Senior et al., 2016; Williams et al., 2015). We find that the magnitude of the global feedback parameter is considerably reduced (i.e., the feedback is less stabilizing) in GC3.1 compared to GC2. This implies a larger equilibrium temperature for a CO_2 doubling, assuming that the linear assumption holds until the system reaches equilibrium. We describe and analyze the reasons for this change to the global feedback, focusing particularly on the cloud radiative feedbacks and their relationship to the many changes made to the cloud parameterizations in the new model. A complete documentation of the coupled feedbacks in GC2 and GC3.1 will be published elsewhere in this special issue, where the ECS of GC3.1 will also be fully documented.

Table 1
List of Model Changes Between GA6.0 and GA7.1 Grouped Into Packages

Name	Package	Ticket numbers/reference
Cnv	Convection	64,84,145
Rad	Radiation	11,16,17
Mic	Microphysics and large-scale precipitation	15, 52, 120
Cld	Large-scale cloud	44,58,89,98,134
Bdl	Boundary layer	13, 83, 162
Dyn	Dynamics	135,146,153,161
Gwd	Gravity wave drag	87,138,151,165
Aer	Aerosols	60
Erf	Effective radiative forcing	Mulcahy et al. (2018)
Sto	Stochastic physics	117
Lnd	Land surface	141,GL tickets: 4,30,31,38,43,45,56

Note. Ticket numbers identify individual model changes, as detailed in Walters et al. (2019). All the tickets are GA tickets, except for the GL tickets in the *Lnd* package. The *Erf* package is documented in Mulcahy et al. (2018).

We use a comprehensive set of present-day and idealized climate change experiments using the atmospheric configurations of the two models to address these issues. These atmosphere-only experiments are known to provide a reliable guide to the atmospheric feedbacks operating in their parent fully coupled model configurations (Gettelman et al., 2012; Ringer et al., 2014). In addition, we also attempt to assess the physical realism of the feedbacks in the two models through comparisons with observed climatologies and variability of cloud processes.

The structure of the paper is as follows. Section 2 describes the model and the experimental set up, and section 3 describes the observational data sets and diagnostic tools used. Section 4 presents the results of the sensitivity experiments carried out to identify the model changes that led to the differences in the feedback parameter. Then, section 5 investigates the mechanisms by which the model changes identified in section 4 affect the feedbacks. A more detailed analysis of the mechanisms related to aerosol-cloud interactions is carried out in section 6. Section 7 discusses the implications of this work, and finally, section 8 summarizes the findings.

2. Model Description and Experimental Setup

The Global Coupled (GC) configurations of the Met Office model contain the following subcomponents: Global Atmosphere (GA), Global Land (GL), Global Ocean (GO), and Global Sea Ice. We use the GA/GL (i.e., atmosphere and land only) simulations to investigate the model changes that led to an increased sensitivity between the two GC configurations. The atmospheric model configurations of GC2 and GC3.1 are GA6.0 and GA7.1, respectively. GA6.0 is coupled to GL6.0, and GA7.1 to GL7.0. For the sake of simplicity, we will refer to the combinations GA/GL simply as GA, appending the corresponding version number. GA6.0 is documented in Walters et al. (2017), and GA7.0 in Walters et al. (2019), and Williams et al. (2018). GA7.1 is an incremental evolution targeting a better representation of the aerosol radiative forcing (Mulcahy et al., 2018).

More than 40 model changes were introduced between GA6.0 and GA7.1, ranging from simple bug fixes to the implementation of an entirely new aerosol scheme. During the testing phase of the development process, the changes were grouped into packages, according to the physical process or scheme to which they belong (Table 1). A detailed description of the model changes that went into these packages is given in Walters et al. (2019), except for the changes between GA7.0 and GA7.1 (*Erf* package), which are described in Mulcahy et al. (2018).

Given the relevance for this study, we give more details of some of the changes here: the new aerosol and mixed-phase cloud schemes, and the *Erf* package. GA7 uses the Global Model of Aerosol Processes (GLOMAP-mode) aerosol scheme described in Mann et al. (2010), which is part of the U.K. Chemistry and Aerosols code. GLOMAP-mode is a two-moment scheme that simulates speciated aerosol mass and num-

ber in four soluble modes and an insoluble Aitken mode. GA6 uses a single-moment scheme, the Coupled Large-scale Aerosol Simulator for Studies in Climate (CLASSIC; Bellouin et al., 2011). The ice phase does not interact with the either of the aerosol representations. Aerosol is not used in ice nucleation and it is not depleted via impaction scavenging by ice. The new mixed-phase scheme was introduced to reduce the Southern Ocean shortwave bias present in previous UM configurations, and common to many climate models (Bodas-Salcedo et al., 2014, 2016a). The scheme parameterizes the role of subgrid-scale turbulence in the production and maintenance of supercooled liquid water (Furtado et al., 2016). The *Erf* package refers to a set of model improvements that targeted the strong, negative aerosol Effective Radiative Forcing found in the GA7.0 configuration. The most relevant changes introduced by this package are new parameterization of the cloud droplet spectral dispersion effect (Liu et al., 2008); multiplicative scaling of the parameterized marine emission of dimethyl sulfide (DMS) by (1 + 0.7), where the factor 0.7 accounts for a missing source of primary marine organic aerosol in GLOMAP-mode; retuning of the Furtado et al. (2016) scheme.

We run all the experiments at N96 horizontal resolution, with an equal-angle grid of 1.875° in longitude and 1.25° in latitude. The atmosphere is divided into 85 layers in the vertical, with the model top at 85 km high. We use boundary conditions and forcings requested by the *amip* experiment of the Coupled Model Intercomparison Project phase 6 (CMIP6; Eyring et al., 2016).

We take advantage of the affordability of atmosphere-only simulations to run a large suite of tests. We use two types of tests: *Off* experiments, where a single package or a combination of them is disabled from GA7.1; and *On* experiments, where a single package or a combination of them is enabled in GA6.0. For example *Mic_On* is a simulation with GA6.0 and the microphysics package from GA7.1 enabled. Since we have two control configurations (GA6.0 and GA7.1), we use the terminology *baseline* for the control configuration to which the changes are applied, and *target* for the other control configuration that defines the changes in the feedbacks to be explained. Therefore, GA6.0 is the baseline configuration for the *On* tests and the target configuration for the *Off* experiments, and vice versa for GA7.1. We use these experiments to decompose the impact of each package on the feedback differences between GA6.0 and GA7.1. The main motivation for using both types of experiments (*On* and *Off*) is to make sure that the effect is qualitatively the same so that the interpretation is robust.

For each test, we run a present-day control (*amip*), and a climate change simulation (*amip-p4K*). The *amip-p4K* experiment is like the *amip*, but with the sea surface temperature increased by 4 K in ice-free ocean (Webb et al., 2017). These types of experiments are relatively inexpensive to run and explain the intermodel spread of atmospheric feedbacks observed in the coupled CO_2-forced counterpart simulations (Ringer et al., 2014).

Since the code changes introduced by all packages are only available in the most recent versions of the UM's code base, it was technically more convenient to start with the tests that use the most recent configuration as baseline, the *Off* tests. The *Off* tests are used as a screening step, to select those model changes that explain most of the difference in λ. They are run for 11 years (January 1979 to December 1989). Then, only a subset of packages is used in the *On* tests, which are run for a longer period of 36 years (January 1979 to December 2014).

3. Observations and Diagnostic Tools

We use a large suite of observational data sets and diagnostics tools to evaluate the realism of the model changes.

The Cloud Feedback Model Intercomparison Project Observation Simulator Package version 1.4 (COSP; Bodas-Salcedo et al., 2011) is run inline to produce model cloud diagnostics that are comparable to the satellite retrievals. We use two of the COSP simulators: the International Satellite Cloud Climatology Project (ISCCP) simulator (Klein & Jakob, 1999), and Cloud-Aerosol Lidar and Infrared Pathfinder Satellite Observations (CALIPSO) simulator (Chepfer et al., 2008). By default, COSPv1.4 uses the Subgrid Cloud Overlap Profile Sampler (Webb et al., 2001) to generate a realistic subgrid cloud vertical overlap. GA6.0 and GA7.1 use different assumptions to produce subgrid variability of cloud condensate (Hill et al., 2011; Walters et al., 2019), and the implementation of COSP has been adapted to account for this.

Table 2
List of Off/On Sensitivity Tests Carried Out, and the Corresponding Global-Mean Feedback Parameters for Net Radiation, SW/LW Clear Sky, and SW/LW Cloud Radiative Effects

Test	λ_{NET}	λ_{SWCS}	λ_{LWCS}	λ_{SWCRE}	λ_{LWCRE}
GA6.0	−1.37	−0.26	2.01	0.84	−0.46
GA7.1	−1.12	−0.34	2.00	1.23	−0.68
Cnv_Off	−1.20	−0.36	2.04	1.07	−0.58
Rad_Off	−1.03	−0.34	1.90	1.27	−0.74
Mic_Off	−1.21	−0.34	1.99	1.09	−0.65
Mic.McICA_Off	−1.04	−0.34	2.01	1.39	−0.75
Mic.WarmRain_Off	−1.15	−0.34	1.98	1.16	−0.66
Mic.MixedPhase_Off	−1.23	−0.35	2.00	1.06	−0.64
Cld_Off	−1.08	−0.35	2.01	1.25	−0.67
Bdl_Off	−1.14	−0.33	1.99	1.19	−0.66
Dyn_Off	−1.20	−0.33	2.06	1.24	−0.71
Gwd_Off	−1.07	−0.35	2.01	1.29	−0.70
AerErf_Off	−1.34	−0.28	2.02	1.06	−0.66
Sto_Off	−1.15	−0.34	2.04	1.18	−0.63
Lnd_Off	−1.14	−0.34	2.01	1.20	−0.67
Erf_Off	−1.12	−0.35	2.01	1.19	−0.66
AerErfMic_Off	−1.38	−0.29	1.99	0.95	−0.63
Aer_On	−1.16	−0.34	2.01	0.98	−0.48
Mic_On	−1.32	−0.28	2.03	0.91	−0.48
AerMic_On	−1.17	−0.34	2.03	1.01	−0.49
AerMicErf_On	−1.09	−0.33	2.02	1.12	−0.52

Note. *Off* experiments use GA7.1 as baseline and revert the package changes back to the GA6.0 configuration. Conversely, the *On* experiments use GA6.0 as baseline and activate the changes introduced by the packages listed in the name. We use upper camel case notation to concatenate package names, for example, *AerMic* is the *Aer* and *Mic* packages combined. A dot is used when a subpackage is used, for example, *Mic.MixedPhase* includes only the mixed-phase changes within the microphysics package. The *Off* experiments were run from January 1979 to December 1989, and the *On* experiments from January 1979 to December 2014. For each test, five global-mean climate feedback parameters ($W{\cdot}m^{-2}{\cdot}K^{-1}$) are listed: net, SW clear sky, LW clear sky, SW cloud effect, and LW cloud effect.

We use the CALIPSO cloud fraction observations from the GCM Oriented Calipso Cloud Product (GOCCP; Chepfer et al., 2010), and the CALIPSO cloud phase observations from Cesana and Chepfer (2013). These observations are provided as monthly averages on a 2° × 2° equal-angle grid. We use v2.9 from June 2006 to December 2015 for the cloud fraction, and v3.1.2 from June 2006 to December 2017 for the cloud phase.

We use three different retrievals of liquid cloud effective radius from the Moderate Resolution Imaging Spectroradiometer (MODIS; King et al., 2003). Level 3 data of the MODIS Collection 6.1 Terra retrievals (Platnick et al., 2015, 2017), from February 2000 to May 2018. Level 3 data of MODIS Collection 5.1 (July 2002 to April 2011) as postprocessed by Pincus et al. (2012), which combines data from the Terra and Aqua satellites into a single product. The third product is the Clouds and the Earth's Radiant Energy System (CERES) Single-Satellite Footprint (SSF) Edition 4 monthly files from the Terra platform (CERES SSF1deg-Month Terra Ed4; Doelling et al., 2013). The three data sets are monthly averages on a 1° × 1° equal-angle grid.

The Multisensor Advanced Climatology (MAC; Elsaesser et al., 2017) algorithm ingests 14 latest version Remote Sensing Systems (gridded, 0.25° × 0.25° Hilburn & Wentz, 2008) data sets for cloud liquid water path, column water vapor, surface wind, and surface rainfall and computes monthly CLWP and total (cloud + rainwater) liquid water path records. The algorithm is described in Elsaesser et al. (2017) and Greenwald et al. (2018). We use monthly mean averages at 1° resolution. For 1° grid boxes, the MAC algorithm corrects for monthly diurnal cycle CLWP biases that arise from averaging over Sun-synchronous input data sets. It

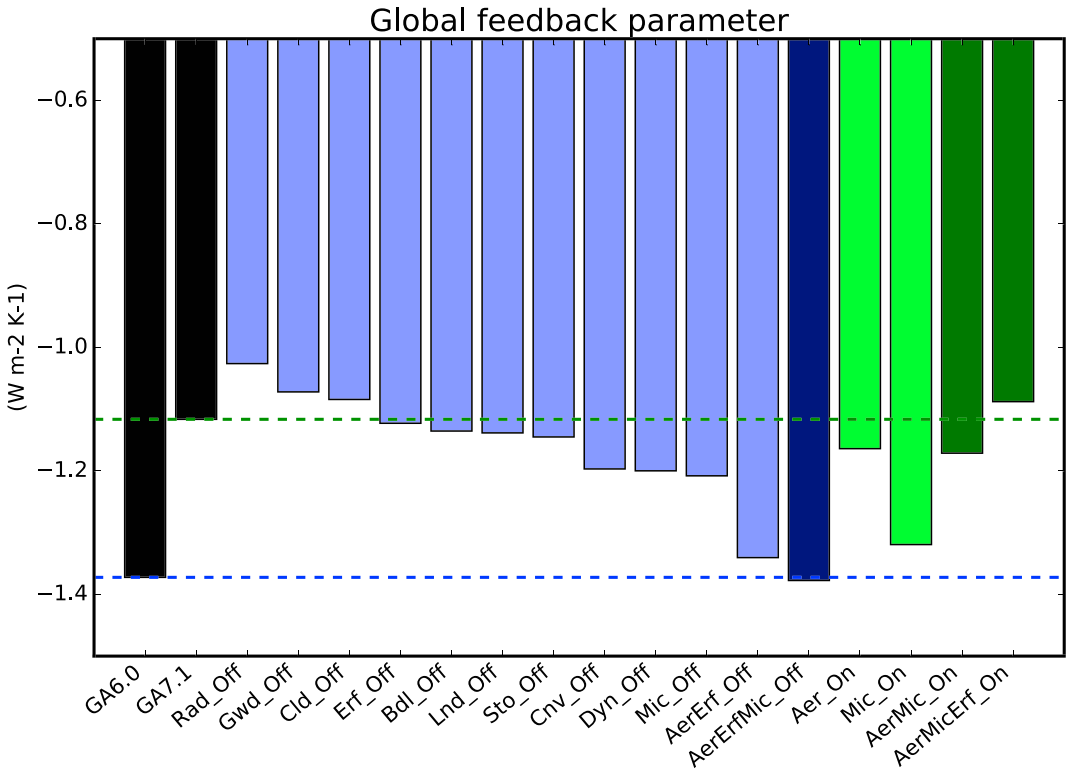

Figure 1. Global-mean feedback parameter. The two control experiments, GA6.0 and GA7.1, are shown in black. The blue bars correspond to the *Off* experiments, and the green bars to the *On* experiments. Each color has two shades: the light shade shows experiments where only one package is changed, and the dark shade when more than one package is changed. Two horizontal lines are shown that serve as the target control experiments: blue for the target of the *Off* experiments (GA6.0), and green for the target of the *On* experiments (GA7.1).

then applies a harmonic regression fit that solves for the monthly mean CLWP, total liquid water path, and climatological diurnal cycles (O'Dell et al., 2008). The cloud LWP statistical uncertainty is estimated to be on the order of 10% over both the middle high latitudes and stratocumulus cloud regimes, and 25% over portions of the ITCZ (Elsaesser et al., 2017). Cloud LWP biases are difficult to quantify; however, variations in assumed drop size distributions, larger-than-expected cloud inhomogeneity over the satellite fields of view and inaccurate partitioning of total liquid water path into cloud and precipitating components may result in biases as large as a factor of 2 over some portions of the tropical oceans (Lebsock & Su, 2014). Such biases are expected to partially cancel during the generation of the monthly and longer-timescale climatologies used in this study.

The following cloud droplet number concentration (CDNC) data sets are used. Grosvenor and Wood (2014) use cloud optical depth and effective radius from Level 2 data of MODIS Collection 5.1 to estimate the liquid CDNC. They use the methodology by Boers et al. (2006) and produce a monthly climatology as described in Grosvenor et al. (2018). The time series used here spans years 2003 to 2014. The second data set is the climatology by Bennartz and Rausch (2017), which uses Level 2 data of MODIS Collection 6.1 from the Aqua satellite from 2003 to 2015. Both data sets are delivered as monthly averages on a $1° \times 1°$ equal-angle grid.

We use the approximate partial radiative perturbation method (APRP; Taylor et al., 2007) to estimate the contributions to shortwave feedback changes from changes in the following properties: surface albedo, clear-sky atmospheric absorption and scattering, and cloud fraction, scattering, and absorption. We apply it off-line to monthly mean model data.

4. Package Testing Results

We use the package testing to select those packages that are the main controls of the change in atmospheric feedbacks between GA6.0 and GA7.1, which we then analyze in detail in the following sections. Table 2 lists the tests that we have carried out: GA6.0, GA7.1, and all the *Off* and *On* experiments.

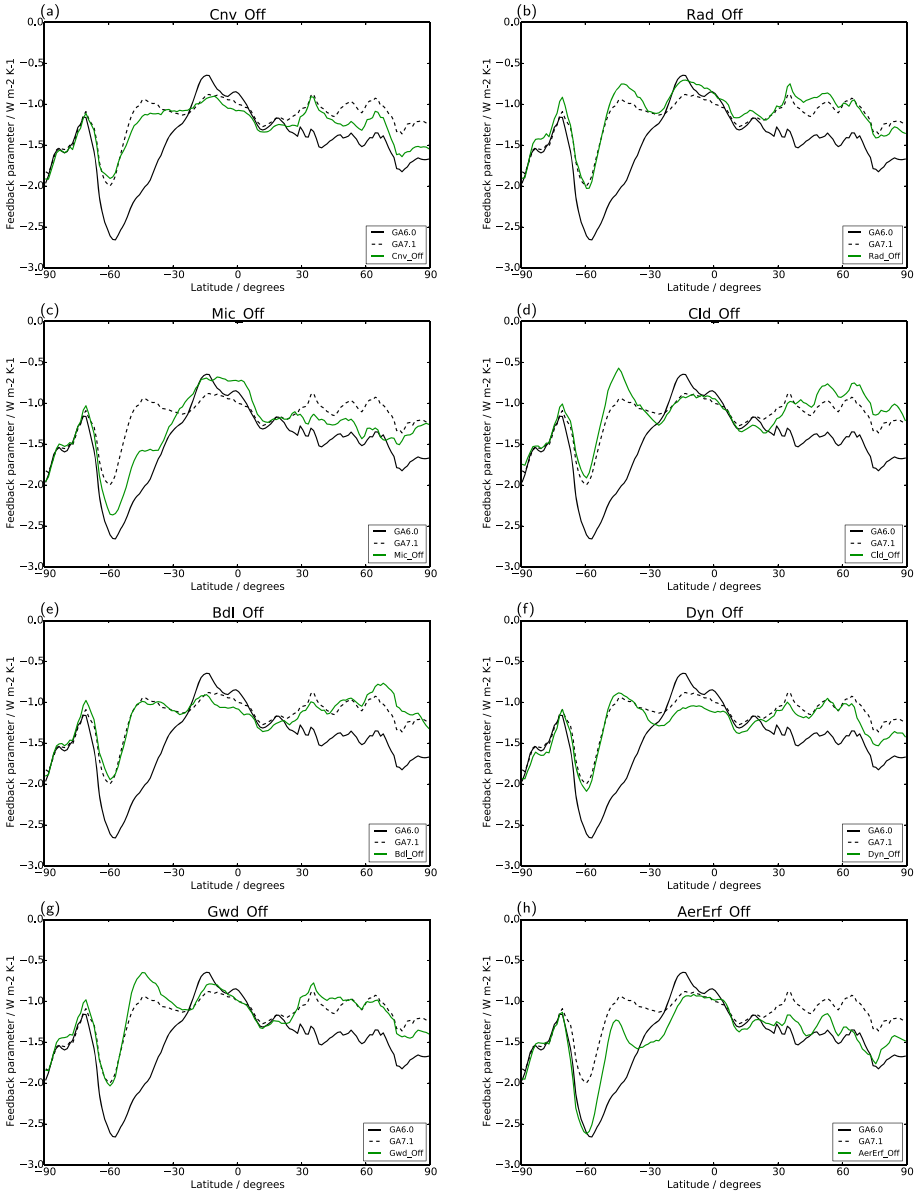

Figure 2. Zonal-mean feedback parameter for the *Off* experiments in which only a single package has been switched off: (a) convection, (b) radiation, (c) microphysics, (d) cloud, (e) boundary layer, (f) dynamics, (g) gravity wave drag, and (h) aerosol and *Erf*. Each plot shows the results for the control experiments in black: GA6.0 (solid) and GA7.1 (dashed). The green, solid line shows the result of the sensitivity experiment. In the *Off* experiments, the closer the green line is to the solid line, the more the experiment explains the changes in zonal-mean feedback parameter.

The feedback parameter, λ, is usually defined as the slope of a linear model of the Earth's temperature response to radiative perturbations (Gregory et al., 2004): $\Delta N = F + \lambda \Delta T_s$. It relates the global-mean net radiation change (ΔN) with the global-mean surface temperature change (ΔT_s), after an initial external radiative forcing (F) is applied to the system. For a stable system, λ is negative. The operator Δ is the difference between the perturbed and the control climates: *amip-p4K* minus *amip*. By construction $F = 0$ in these experiments, and therefore, the global-mean feedback parameter is calculated as $\lambda = \Delta N / \Delta T_s$ (Cess et al., 1990).

We first look at the change in global-mean feedback parameter in the *Off* tests (Figure 1). For the *Off* tests, the blue dashed line shows the value of the target experiment (GA6.0). Of all the single-package tests, *AerErf_Off* by itself explains most of the change in global-mean feedback parameter. We treat *AerErf* as a single package in the *Off* tests because *Aer* cannot be disabled without disabling part of *Erf*. It is worth mentioning that aerosol emissions are unchanged in the *amip-p4K* experiments.

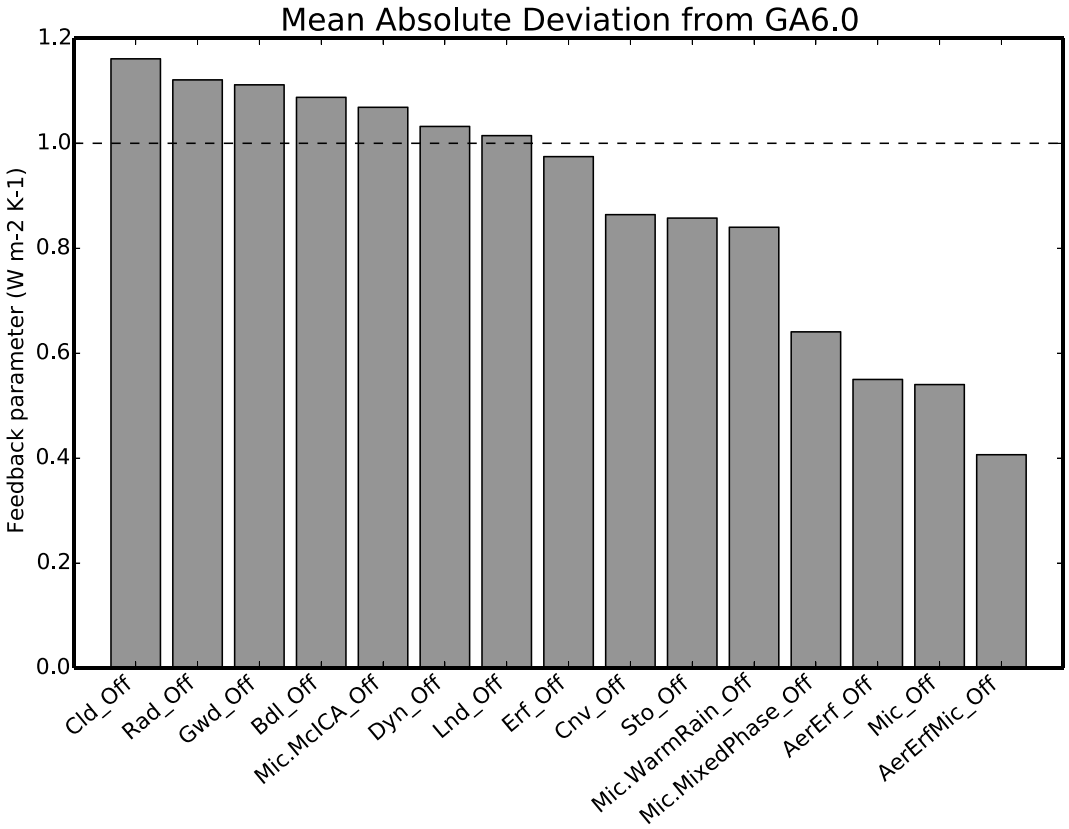

Figure 3. Normalized mean absolute deviation of the net feedback parameter. It is calculated with respect to GA6.0, and normalized by the value of GA7.1.

There are three other packages that change the feedback parameter toward the target line: *Cnv_Off*, *Mic_Off*, and *Dyn_Off*. The remaining packages only introduce either small changes in the global-mean feedback parameter or they move it away from the target configuration.

The global-mean feedback parameters for the control experiments are (Table 2): $-1.37\ \mathrm{W{\cdot}m^{-2}{\cdot}K^{-1}}$ for GA6.0, and $-1.12\ \mathrm{W{\cdot}m^{-2}{\cdot}K^{-1}}$ for GA7.1. Adding the effect of all the *Off* experiments (except *Erf_Off*, which is already included in *AerErf_Off*) would give a global-mean value of $-1.50\ \mathrm{W{\cdot}m^{-2}{\cdot}K^{-1}}$. The large residual with respect to GA6.0 implies that, unsurprisingly, the packages interact in a nonlinear fashion.

Zonal-mean averages of the feedback parameter offer greater insight into the packages that dominate the changes in the feedback parameter (Figure 2). Generally, GA7.1 shows a less strong negative feedback in the midlatitudes in both hemispheres, and at high latitudes in the Northern Hemisphere. *AerErf_Off* explains a substantial amount of the zonal pattern changes, consistent with the global-mean results. *Cnv_Off* and *Dyn_Off* generally show a slightly more negative feedback parameter than in the control experiment, but none of them seem to produce a zonal-mean pattern that is closer to the target experiment, apart from the Northern Hemisphere high latitudes, where *Cnv_Off* does get substantially closer to GA6.0. *Mic_Off* is a very interesting case: the zonal pattern gets substantially closer to GA6.0 nearly everywhere, but due to cancellation of positive (tropics) and negative (extratropics) differences with respect to GA7.1, the change in the global-mean value is similar to *Cnv_Off* and *Dyn_Off* (Figure 1). These results strongly suggest that the new aerosol scheme and changes in the microphysics explain most of the change in atmospheric radiative feedbacks between GA6.0 and GA7.1.

The area-averaged mean absolute difference (MAD) is a metric that does not suffer from the compensating effects that affect the global-mean differences in Figure 1. For each *Off* test, we calculate this metric by taking the absolute value of the zonal-mean differences of the feedback parameter between the test and GA6.0. The MAD is then calculated as the area-weighted mean of these differences. We then normalize the results by the MAD value of GA7.1. Values smaller than 1 imply that the test produces zonal means closer to GA6.0.

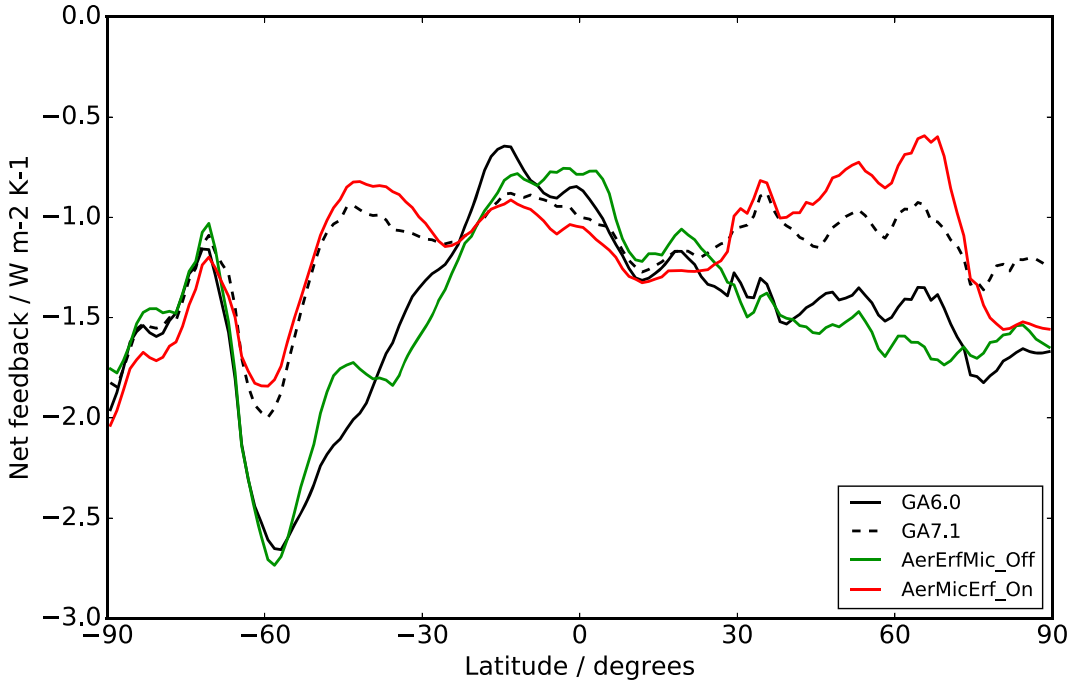

Figure 4. Impact in the zonal-mean feedback parameter for the tests *AerErfMic_Off* and *AerMicErf_On*. The control experiments are the black lines: GA6.0 (solid) and GA7.1 (dashed). The green and red solid line shows the result of the sensitivity experiments. The closer the green (red) line is to the black solid (dashed) line, the more the experiment explains the changes in zonal-mean feedback parameter.

Figure 3 clearly shows that *AerErf_Off* and *Mic_Off* are the two single-package tests that substantially reduce the MAD, in agreement with our visual interpretation of the zonal-mean plots in Figure 2.

When we combine the effect of the *AerErf* and *Mic* packages (*AerErfMic_Off*), the zonal-mean feedback parameter follows very closely that of GA6.0 (Figure 4). This shows that, zonally, these two packages interact in a relatively linear fashion. They explain most of the changes in the extratropics, perhaps making the feedback parameter too negative as compared to GA6.0. In the tropics, the differences between GA6.0 and GA7.1 are not big enough for the zonal means to be informative.

We confirm the results obtained by the *Off* experiments by running *On* experiments for the packages *Aer*, *Mic*, *AerMic*, and *AerMicErf* (green bars in Figure 1). The global-mean feedback parameter shows a big change toward the target control experiment (GA7.1) for *Aer_On*, and a much smaller change toward GA7.1 for *Mic_On* due to the compensating effects mentioned above. The combined package *AerMicErf_On* has a global feedback parameter very close to GA7.1, slightly less negative, confirming the nearly symmetric behavior of these packages in the global-mean sense in the *Off* and *On* tests. This nearly symmetric behavior is confirmed by the *AerMicErf_On* zonal mean in Figure 4.

We investigate in more detail the impact of the microphysics package by splitting it into three independent changes. The first subpackage implements upgrades to the Monte Carlo Independent Column Approximation (McICA; Pincus et al., 2003) by introducing a new parametrization that links the characteristics of the subgrid cloud horizontal variability and vertical overlap to the model resolution and cloud fraction in the grid box (Walters et al., 2019). The second subpackage makes significant changes to the representation of warm rain in the microphysics scheme (Boutle & Abel, 2012; Boutle et al., 2014). The third subpackage implements a new scheme that accounts for turbulent production of liquid water in mixed-phase clouds (Furtado et al., 2016). We have labeled these subpackages as *Mic.McICA*, *Mic.WarmRain*, and *Mic.MixedPhase*, respectively. Figure 3, and analysis of zonal means of the feedback parameter (not shown), shows that the *Mic.MixedPhase* subpackage is the leading contributor to the *Mic* package, although the contribution of the *Mic.WarmRain* subpackage is nonnegligible. The *Mic.MixedPhase* subpackage was introduced to reduce the Southern Ocean shortwave bias present in previous UM configurations (Hyder et al., 2018; Walters et al., 2019). Until recently, this bias has been common to many climate models, due to the lack of supercooled

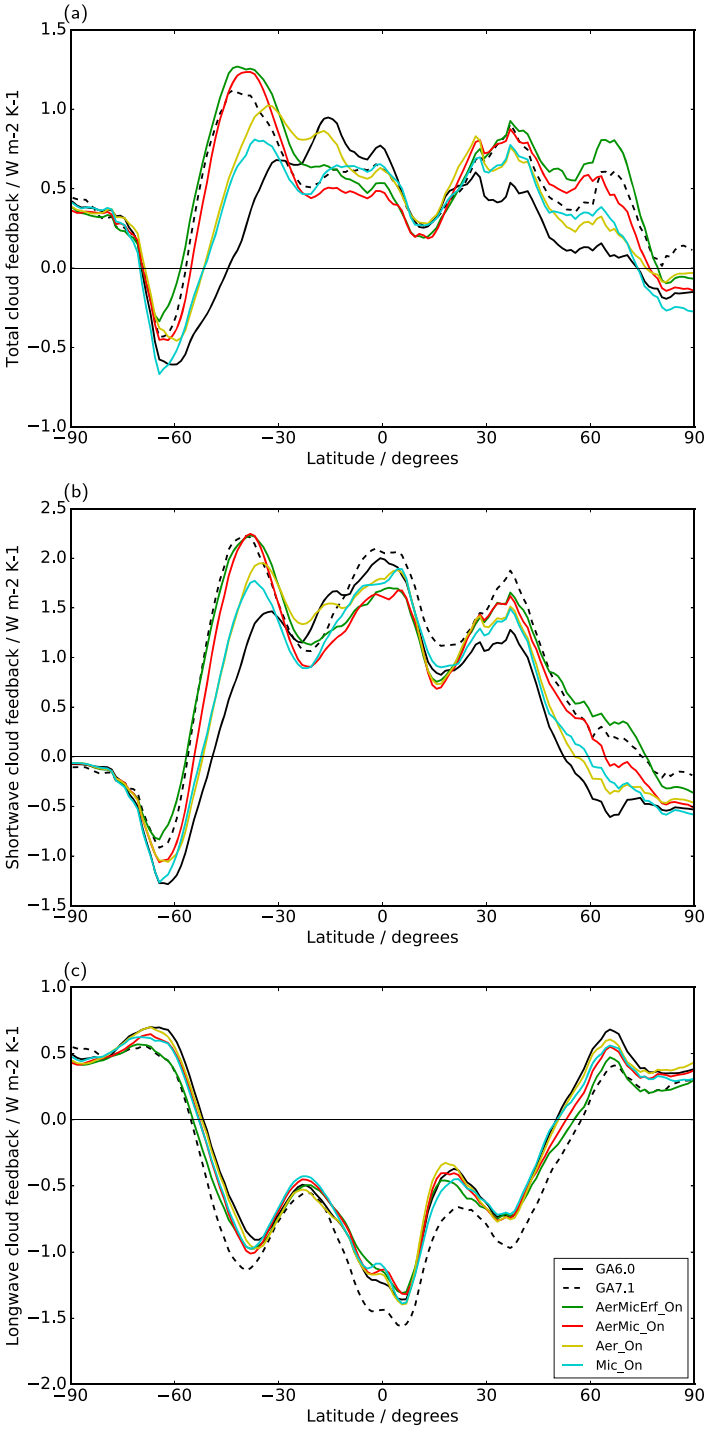

Figure 5. Impact on the zonal-mean feedback parameter of the *On* packages: (a) total, (b) shortwave, and (c) longwave cloud feedbacks. The control experiments are the black lines: GA6.0 (solid) and GA7.1 (dashed). The colored solid lines show the result of the sensitivity experiments. The closer the sensitivity test line is to the black dashed line, the more the experiment explains the changes in zonal-mean feedback parameter.

Table 3
Regional-Mean Contributions to Changes in SW Feedback Using the APRP Method

	Clear scattering	Cloud	Cloud amount	Cloud scattering
30–50°S				
GA6.0	*−0.07*	*0.67*	*0.96*	*−0.22*
GA7.1	-0.00	0.96	0.33	0.63
AerMicErf_On	0.01	0.99	0.25	0.76
AerMic_On	0.01	0.87	0.21	0.68
Aer_On	0.03	0.52	0.07	0.46
Mic_On	-0.01	0.40	0.16	0.24
50–70°S				
GA6.0	*−0.26*	*−1.07*	*0.23*	*−1.23*
GA7.1	0.17	0.79	0.13	0.66
AerMicErf_On	0.17	0.84	0.13	0.74
AerMic_On	0.19	0.54	0.04	0.52
Aer_On	0.20	0.31	0.02	0.30
Mic_On	0.01	0.22	0.01	0.22

Note. The first row for each region shows the actual feedback contributions for GA6.0 (in italic), whereas all the other rows show the differences with respect to GA6.0. Only the dominant terms are shown: clear-sky scattering and cloud (split into cloud amount and cloud scattering). APRP = approximate partial radiative perturbation method.

liquid cloud (Bodas-Salcedo et al., 2014, 2016a). The improvement in the simulation of supercooled liquid cloud is expected to reduce the strength of the negative optical depth feedback in the Southern Ocean (Tan et al., 2016), although the effect of the reduction of this bias may depend on the climatology of cloud vertical structure of each model (Bodas-Salcedo, 2018; Lohmann & Neubauer, 2018).

Figure 5 shows the zonal means of the net cloud feedback and its decomposition into SW and LW components for the two baseline experiments and for combinations of the *Mic_On*, *Aer_On*, and *Erf_On* packages. The net cloud feedback shows a similar pattern of changes to the feedback parameter between GA6.0 and GA7.1 (Figure 5a), and this pattern is mainly dominated by the SW component (Figure 5b). The LW component in GA7.1 shows a nearly constant shift towards more negative values nearly everywhere (Figure 5c). It balances the more positive SW component in the tropics, especially in the Northern Hemisphere.

We can then conclude that the SW cloud feedback is the leading component that controls the net feedback differences between GA6.0 and GA7.1. Two main model developments are responsible for these changes: mixed-phase cloud and aerosol schemes. From now on, we focus on the analysis of the *On* experiments for a combination of a subset of packages: *Aer*, *Mic*, and *Erf*.

5. Controls of Feedback Differences

The analysis above has shown that the midlatitudes are responsible for most of the feedback differences between GA6 and GA7.1. We now focus on understanding which changes in cloud properties drive the differences in feedback in the Southern Ocean (30–70°S). We restrict our analysis to the Southern Ocean for simplicity because of its zonally symmetric behavior, without losing too much generality: the Northern Hemisphere midlatitudes show changes that are qualitatively similar. In GA6.0, the Southern Ocean region transitions from a positive SW feedback between 30°S and 50°S, to a negative SW feedback between 50°S and 70°S. As we show below, the characteristics of the feedback differences in these subregions are different, so we present results for both regions independently.

Table 3 shows the partition of the SW feedback into different contributions, as estimated by the APRP method (Taylor et al., 2007). The residual terms are small (less than 0.05), giving confidence in this partition. Cloud optical depth drives the feedback changes between GA6.0 and GA7.1 in both regions, although the cloud fraction contribution is not negligible, and it is important in the region between 30°S and 50°S. Incidentally, this coincides with a dominant cloud fraction component in 30–50°S and a dominant optical depth component in 50–70°S in GA6.0. The region between 30°S and 50°S shows a stronger change in cloud feed-

back between GA6.0 and GA7.1, with changes in optical depth contributing with two thirds of the total, and changes in cloud fraction the remaining third. The feedback differences in the 50–70°S region are mostly attributed to changes in cloud optical depth.

The microphysics package is responsible for most of the cloud fraction feedback change between 30°S and 50°S (Table 3). The aerosol package dominates the optical depth changes, with the microphysics also contributing significantly, with 30% to 40% of the optical depth changes. It is interesting to note that the new aerosol scheme largely suppresses a strongly negative clear-sky feedback present in GA6.0 between 50°S and 70°S.

The *Erf* package cannot be applied independently, as it builds on top of the *Aer* and *Mic* packages. Although it does affect the feedback changes of both the microphysics and aerosols schemes, it seems that its main contribution is through the enhancement of the effects of the microphysics because it shows a significant cloud fraction and LWP effects (Table 3).

Figure 6 shows the seasonal cycles for COSP/CALIPSO low cloud fraction (top row), cloud liquid water path (middle row), and cloud top effective droplet radius (bottom row). The left-hand column shows results for 30–50°S, and the right-hand column for 50–70°S. Figures 6a and 6b show that the cloud fraction feedback is mainly operating in the region between 30°S and 50°S, in agreement with the APRP results. GA7.1 cloud fraction shows better agreement with the GOCCP observations, although it is still biased low.

The behavior of LWP and cloud effective droplet radius inform about the optical depth contributions to the change in feedback (Figures 6c–6f). GA7.1 shows more LWP in the climatology in both regions, in closer agreement with the MAC LWP observations, although it is still biased low between 50°S and 70°S. MAC cloud LWP is possibly 5–10% biased high over these latitudes, largely due to an overestimation of the amount of liquid in the column that is partitioned as cloud versus the precipitation/drizzle category (Greenwald et al., 2018). Removing this bias would bring GA7.1 closer to the observations, except during winter in the lower midlatitudes. Between 30°S and 50°S, GA7.1 shows a suppressed LWP response, with even a decrease in LWP between December and May. The microphysics package is the main contributor to the LWP changes. In the region between 50°S and 70°S, the LWP response of GA7.1 is very similar to GA6.0 (Figure 6d). The *Mic* and *Erf* packages reduce the response, but this reduction must be compensated by other packages or interactions between them to give a very neutral change in GA7.1. The changes in the LWP climatology are mainly due to the tuning of the mixed-phase scheme included in the *Erf* package (Mulcahy et al., 2018; Walters et al., 2019), which doubles the vertical length scale over which the turbulence is assumed to mix in the new mixed-phase scheme. It is worth noting that this tuning sets the vertical length scale back to the value originally recommended by Furtado et al. (2016). Increasing it will increase the production of supercooled liquid water cloud by turbulence. Both the increase of climatological LWP and the suppressed or neutral response (with respect to GA6.0) contribute to the positive changes in SW feedback.

The behavior of the cloud droplet effective radius is qualitatively similar in both regions (Figures 6e and 6f). GA7.1 has climatologically smaller cloud droplets, and it shows a small increase in droplet size with warming. GA6.0 shows strong seasonal cycles, both in the climatology and in the response, whereas GA7.1 shows virtually no seasonal dependency. The *Aer* package and the *Erf* packages explain all the differences between GA6.0 and GA7.1. The effect on the SW feedback is dominated by the summer months, where the insolation is stronger. In these months, GA6.0 shows a large reduction in droplet size with warming, which will produce a negative SW feedback. This negative feedback is completely suppressed or even positive in GA7.1, which shows a small increase in droplet size with warming. The MODIS observations show larger cloud droplet sizes than the models in the present-day climate during the summer months. We do not show the Pincus et al. (2012) climatology in these plots because it is virtually identical to the MODIS C6.1 climatology. The CERES climatology provides retrievals from different combination of channels. We have used the daytime product that uses the 1.2-μm channel because this product reports the largest droplet sizes, providing an estimate of the structural uncertainty in the retrievals. It seems evident that satellite retrievals in these latitudes are still very uncertain and can be subject to large biases. Liang et al. (2015) show that MODIS retrievals can be biased high by as much as 7 μm in the Southern Hemisphere midlatitudes, which makes the assessment of the realism of the model changes challenging. Despite these uncertainties, the results suggest that both configurations underestimate the droplet size in the present day, but GA7.1 does so more dramatically.

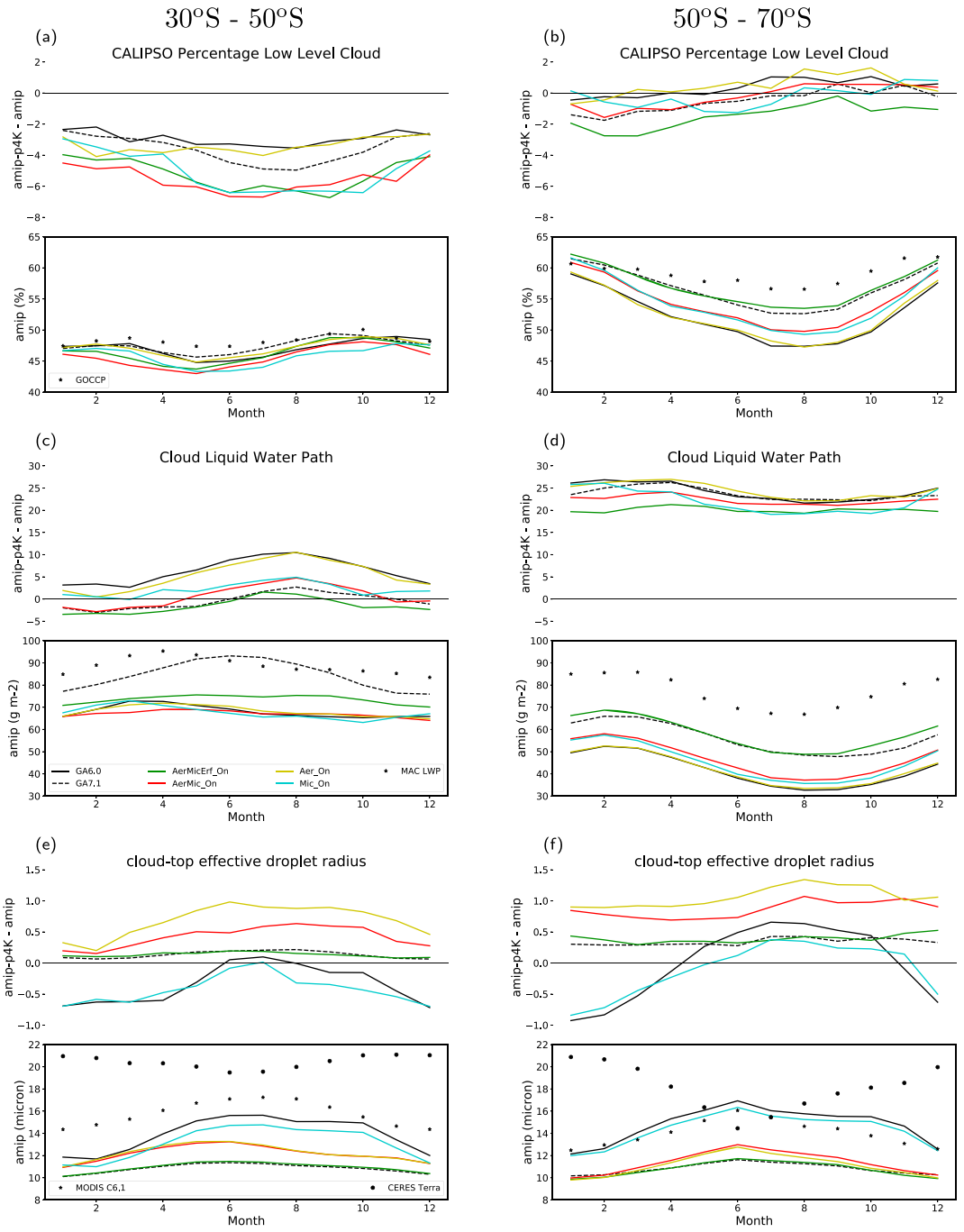

Figure 6. Seasonal cycles for COSP/CALIPSO low cloud fraction (a, b), cloud liquid water path (c, d), and cloud top effective droplet radius (e, f). The left-hand column shows results for 30–50°S, and the right-hand column for 50–70°S. Each plot contains two subplots: the control climatology at the bottom, and the *amip-4K* minus *amip* response at the top.

It is worth highlighting the role of the LWP and droplet size climatologies on the feedback. In both cases, the changes in the climatologies between GA6.0 and GA7.1 contribute toward brighter clouds, which will enhance the strength of the existing cloud fraction feedback. That is, the radiative perturbation per change in unit cloud depends on the albedo of the control cloud climatology. Because of changes in the climatology of LWP and droplet size, the cloud fraction feedback between 30°S and 50°S (Figure 6a) will be more positive in GA7.1. In addition to this, the strength of the albedo feedback also depends on the base state, with the change in cloud albedo being controlled by the fractional differences of LWP and droplet size, not their absolute

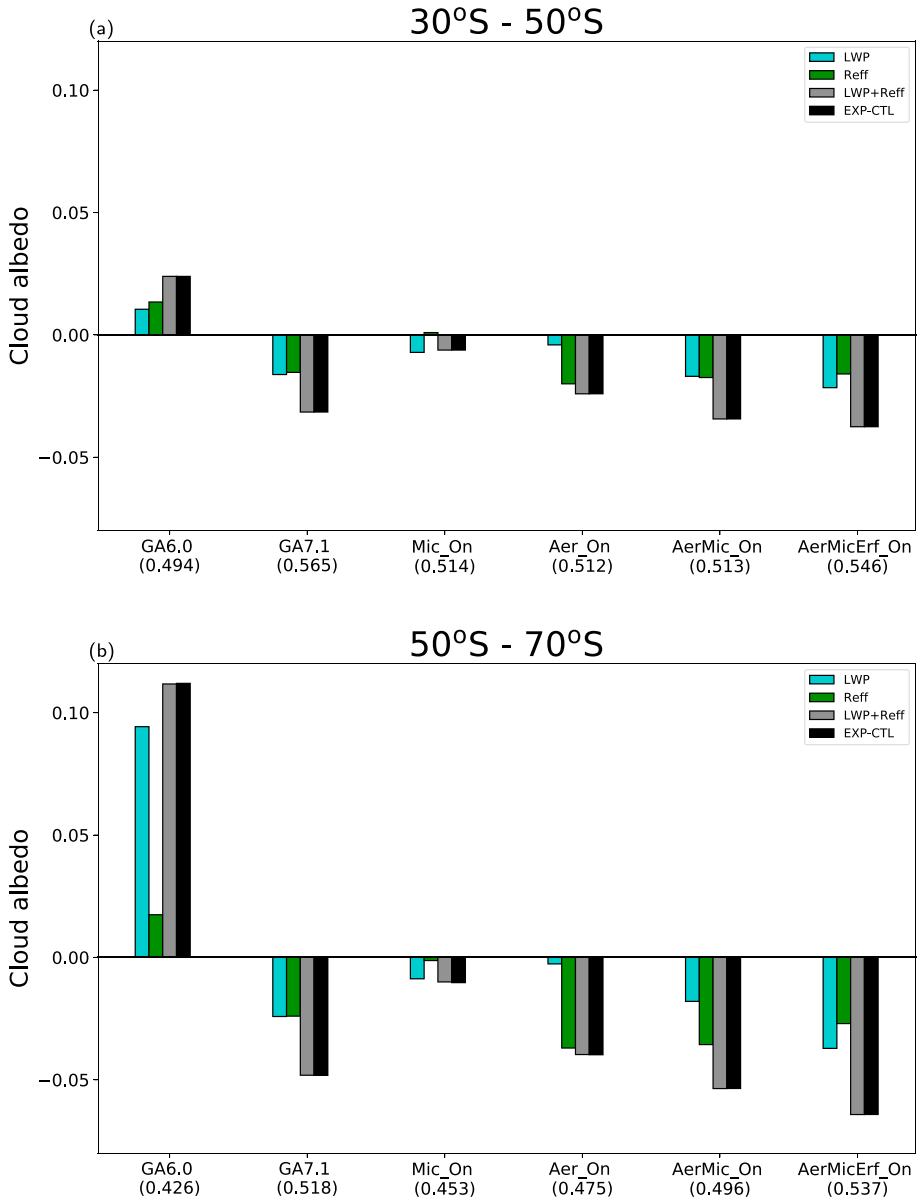

Figure 7. Estimates of contributions to cloud albedo changes with warming for climatological January in two regions: (a) 30–50°S, and (b) 50–70°S. The cloud albedo feedback (*amip-p4K* minus *amip*) is in black, and the contributions from LWP in cyan, from cloud droplet size in green, and their linear combination in gray. The GA6.0 results are actual albedo changes, whereas the others show differences with respect to GA6.0. The numbers in parentheses are the climatological cloud albedos for the *amip* experiments. LWP = liquid water path.

changes. In this respect, the changes in LWP climatology tend to reduce the efficiency of the LWP-mediated negative feedback in GA7.1, whereas the changes in the droplet size climatology enhance the efficiency of the feedback. In both cases, the climatological changes contribute toward a positive differential change in SW feedback.

Figure 6 shows that the qualitative interplay between the changes in cloud radiative properties and their effect on the SW feedback is complex. In order to understand these relationships in a more quantitative manner, we have estimated the contributions from LWP and droplet size to change in cloud albedo using the following simple approach: the cloud albedo, α, is a function of the cloud optical depth (τ) and is calculated using the parametrization used in the ISCCP simulator (Klein & Jakob, 1999): $\alpha = \tau^{0.895}/(\tau^{0.895} + 6.82)$. This equation is an analytical approximation to the lookup tables used by the ISCCP operational processing (Rossow & Schiffer, 1999). The cloud optical depth is calculated as $\tau = (1.5/\rho)LWP/R_{eff}$ (Stephens, 1978),

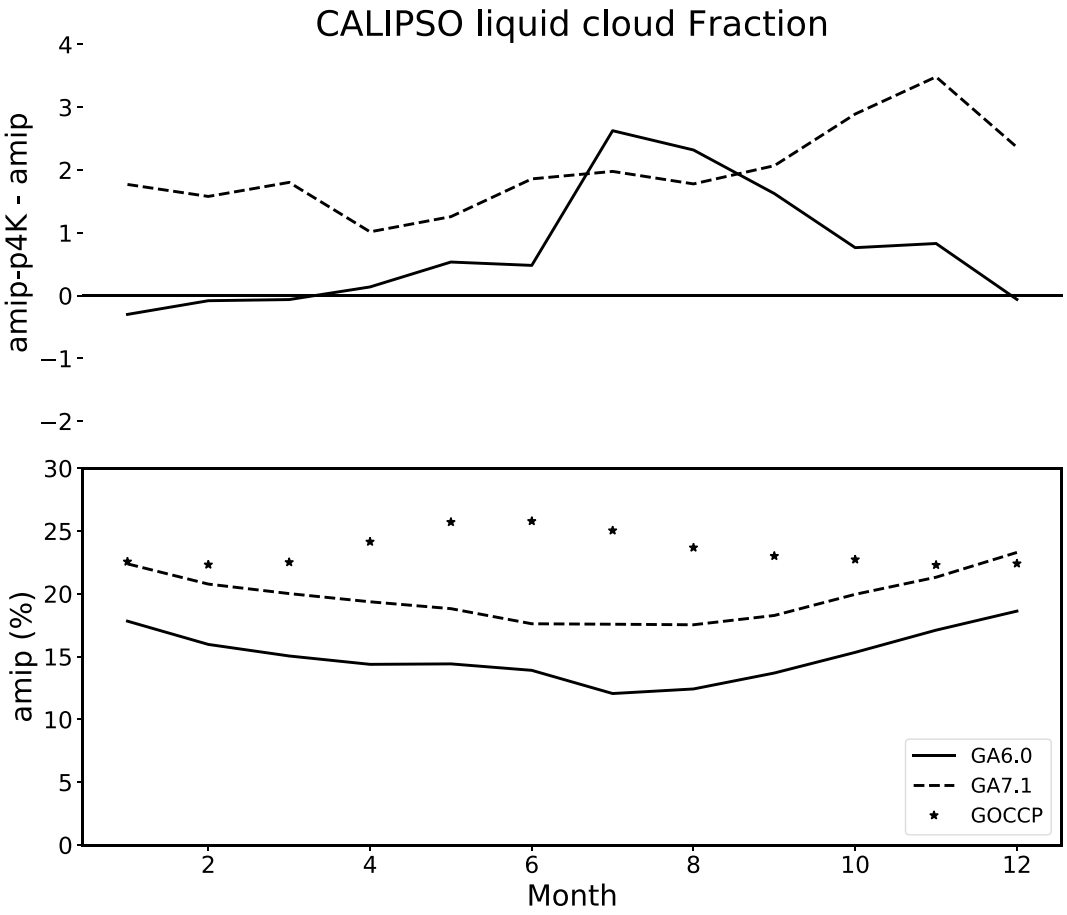

Figure 8. Seasonal cycles for COSP/CALIPSO liquid cloud fraction at 720-m altitude for the region between 50°S and 70°S. Control climatology shown in the bottom plot, and the *amip-4K* minus *amip* response at the top. Two model configurations are shown: GA6.0 and GA7.1. GOCCP observational climatology is also displayed.

with ρ being the density of liquid water. Then, four calculations are done for each grid box, using monthly averages as inputs:

- LWP: $\alpha(LWP^{amip-p4K}, R_{eff}^{amip}) - \alpha(LWP^{amip}, R_{eff}^{amip})$,
- R_{eff}: $\alpha(LWP^{amip}, R_{eff}^{amip-p4K}) - \alpha(LWP^{amip}, R_{eff}^{amip})$,
- LWP+R_{eff}: sum of the two calculations above,
- EXP-CTL: $\alpha(LWP^{amip-p4K}, R_{eff}^{amip-p4K}) - \alpha(LWP^{amip}, R_{eff}^{amip})$.

These calculations estimate the contributions from changes in LWP, droplet size, linear combination of LWP plus droplet size, and total change, respectively. Although we do not expect these calculations to be an accurate estimate to the true model cloud albedo, they provide useful quantitative information for the interpretation of the differences in the SW cloud feedback.

Figure 7 shows results for January, representative of a summer month with large insolation. It shows the contributions to the difference in cloud albedo as described above, and the mean albedo for the *amip* experiment is displayed in parentheses under axis labels. To facilitate the interpretation, the bars for GA7.1 and the package tests show the differences in cloud albedo with respect to GA6.0. For these, zero change means that its absolute change in cloud albedo is equal to that in GA6.0. The GA6.0 bars show the actual *amip-p4K* minus *amip* changes.

The first thing to note about the results in Figure 7 is that the linear decomposition is very accurate: the gray bars in the top plot are always nearly identical to the black bars. Second, the behavior of the total contribution (EXP-CTL) is consistent with the APRP results for cloud scattering, albeit with some differences

in the details. Since these two methods are independent, this gives us confidence in the utility of Figure 7 to understand the mechanisms driving the changes.

GA7.1 and the package tests show very similar behavior in both regions. The microphysics package contributes to a positive change in feedback mainly through changes in LWP, whereas the aerosol scheme operates mainly through the droplet size. *AerMic_On* shows a combination of both effects. The *Erf* changes enhance the LWP changes of the microphysics and suppresses some of the droplet size effect of *Aer*. These two effects are consistent with two independent changes introduced by *Erf*: increase of the effect of the mixed-phase scheme by increasing of the vertical mixing length scale; weakening of the dependency of cloud droplet size with LWP and aerosol number concentration with the implementation of the Liu et al. (2008) spectral dispersion scheme. Although qualitatively both regions are very similar, the region between 50°S and 70°S shows larger changes in GA7.1 and in the package tests. In both regions, LWP and droplet size changes contribute equally to the change in feedbacks, but the LWP feedback is much stronger to start with in the region between 50°S and 70°S.

Figure 7 also displays the different characteristics of the baseline model (GA6.0) feedbacks in these two regions. Consistent with the APRP method (Table 3), GA6.0 shows a moderate negative feedback (increase in cloud albedo) between 30°S and 50°S, and a much stronger negative feedback between 50°S and 70°S. Figure 7 shows that the droplet size component is similar in both regions, and the difference is due to a much stronger LWP feedback between 50°S and 70°S, where supercooled liquid clouds play a large role in the SW radiation in the real world (Bodas-Salcedo et al., 2016a).

Previous studies have suggested that, as models improve the representation of supercooled liquid cloud in this region, the strength of this negative feedback should decrease (Bodas-Salcedo et al., 2016b; Tan et al., 2016), consistent with the effects of the *Mic* package in Figure 7b: the reduction of the LWP radiative feedback is bigger when the climatological albedo is larger. Figure 8 shows the seasonal cycles for liquid cloud fraction from the COSP/CALIPSO simulator between 50° and 70°S. The results are for a layer centered at 720 m of altitude. GA7.1 shows a substantial increase in the climatology of liquid cloud fraction, bringing it closer to the observations, which supports the hypothesis that a better representation of supercooled liquid cloud should lead to a reduction in the negative SW feedback in this region. However, this response is not necessarily robust across models (Lohmann & Neubauer, 2018).

6. Aerosol-Cloud Interactions

The analysis above shows that the microphysics changes are responsible for changes in the LWP feedback, and the new aerosol scheme is responsible for the droplet size feedbacks. In this subsection we are going to investigate in more detail the mechanisms that control the droplet size feedback. The Southern Ocean is one of the most pristine aerosol regions in the world (Hamilton et al., 2014) where aerosols are predominantly natural in origin, namely, coming from sea-spray and marine emissions of primary organic matter and gaseous dimethyl sulfide (DMS). Once in the atmosphere gaseous DMS is oxidized and eventually forms sulfate aerosol. We restrict the analysis to the region between 50°S and 70°S because the DMS seasonal cycle is stronger, which makes the analysis clearer, but the conclusions can be extended to the other region. The satellite retrievals of CDNC are less reliable between 50°S and 70°S, but nonetheless, the models show qualitatively similar biases in both regions.

Several aspects of the new aerosol scheme can potentially impact the number of particles activated into cloud droplets and therefore the cloud droplet size: primarily the dynamic evolution of the aerosol size distribution via the simulation of both aerosol number as well as mass, inclusion of aerosol microphysics processes, such as coagulation, nucleation, condensation, cloud processing (Mann et al., 2012) and a more sophisticated treatment of aerosol activation into cloud droplets (West et al., 2014). Focusing on species predominant over the Southern Ocean there are updates to the seawater concentration of DMS, new emission parametrizations for both sea spray and DMS, a prognostic treatment of sea salt aerosol, and differences in the aqueous phase sulfur chemistry. We now assess the importance of some of these processes as controlling factors in the change in feedbacks between the two model configurations.

Figure 9 shows that the climatological seasonal cycle in CDNC at cloud top peaks in January, with a minimum during the winter months. GA6.0 shows a larger amplitude than GA7.1. The climate change response in GA6.0 shows a large seasonal cycle and is nearly null in GA7.1. The new aerosol scheme is responsible

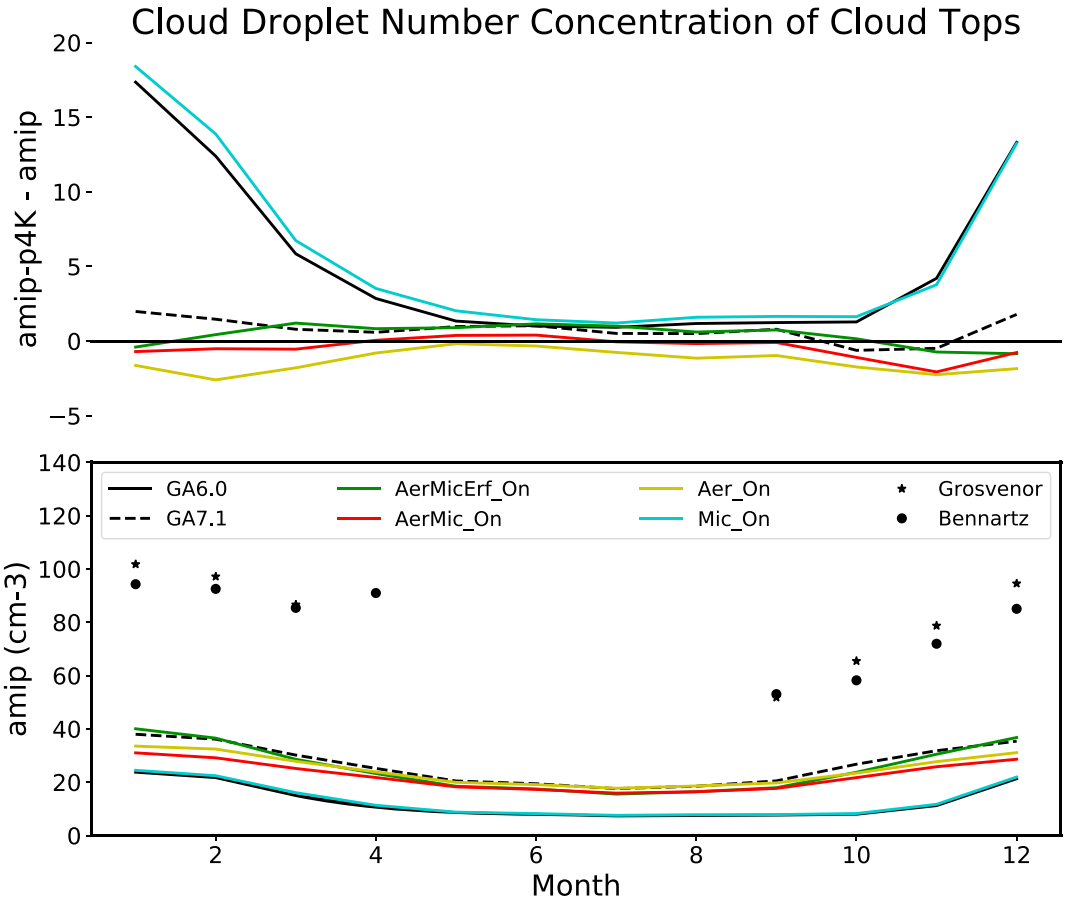

Figure 9. Seasonal cycles for cloud droplet number concentration at cloud top for the region between 50°S and 70°S. Control climatology shown in the bottom plot, and the *amip-4K* minus *amip* response at the top.

for the change in behavior. Comparison with Figure 6f strongly suggests that CDNC controls the seasonal cycle of droplet size, with variations in LWP potentially playing a small role. Despite the increase in CDNC, GA7.1 is still biased low with respect to the satellite retrievals. The biases are smaller in the region between 30°S and 50°S (not shown), where the observations are more reliable, but both models still show a consistent low bias. To avoid large sampling biases in the observations due to lack of retrievals in the higher latitudes of the domain during the winter months, we show observational data only for months where the percentage of grid boxes with missing data is less than 60%. It is difficult to reconcile these results with the droplet size comparisons presented above (Figure 6f). A low bias in both CDNC and droplet size of the magnitude that the models show should result in a low bias in LWP of at least an order of magnitude, assuming constant cloud properties in the vertical. This is not what the comparisons against independent microwave LWP observations show (Figure 6d). This inconsistency suggests that the droplet size and CDNC retrievals, which are not independent, are subject to large uncertainties.

Over the Southern Ocean, sea salt and DMS are significant aerosol sources that contribute to CDNC in both model configurations. In GA7.1, the marine DMS emissions are scaled by 1.7 to represent the missing marine organic source (Mulcahy et al., 2018). The seasonal cycle of the sea-salt contribution to CDNC is in opposite phase with respect to that of DMS (Mulcahy et al., 2018), so it cannot explain the seasonal cycle of CDNC. We therefore conclude that DMS is the primary controller of the CDNC seasonal cycles observed in Figure 9.

GA7.1 replaces not only the aerosol scheme but also the seawater concentration of DMS and the emission parametrization that calculates the sea-to-air flux of DMS. All these changes are included in the *Aer* package. We now look into the role of these different aspects of the DMS cycle and their impact on the CDNC response.

GA6.0 uses the Kettle et al. (1999) climatology of DMS concentration in sea water, whereas GA7.1 uses a more recent climatology by Lana et al. (2011). The Kettle et al. (1999) climatology has a much stronger

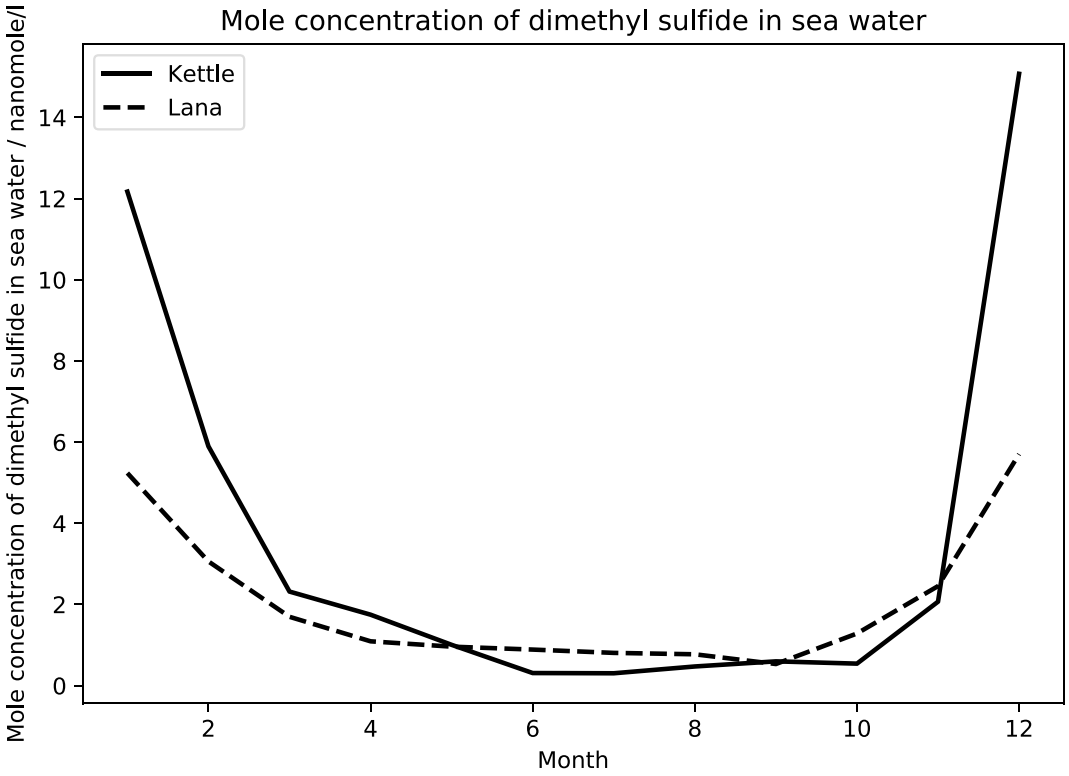

Figure 10. Seasonal cycle of DMS concentration in sea water for the Kettle et al. (1999) climatology used in GA6.0, and for the Lana et al. (2011) climatology used in GA7.1. Regional averages between 50°S and 70°S.

seasonal cycle than the Lana et al. (2011) climatology (Figure 10). Reduced DMS concentrations in the high polar latitudes are due to the inclusion of a significantly increased number of observations and improved spatial coverage in the Lana et al. (2011) climatology .

If we follow the pathway from DMS concentration in sea water to its contribution to CDNC, the next aspect that has changed is the emission parametrization. GA6.0 uses the Wanninkhof (1992) parametrization, and GA7.1 uses the one proposed by Liss and Merlivat (1986). Both parametrize the DMS mass transfer velocity over sea as a function of wind speed and the Schmidt number. The calculation of the Schmidt number as a function of surface temperature is shared by both schemes, so the differences are through their dependency on wind speed. Figure 11 shows the seasonal cycle of DMS emissions using the four possible combinations of DMS concentration in seawater and emission parametrization. The calculations have been done off-line, using monthly mean inputs from the GA6.0 *amip* and *amip-p4K* simulations. It is clear that the Kettle-Wanninkhof GA6.0 is the one that produces the stronger seasonal cycle, both for the control and for the climate change response, even after applying the 1.7 scaling factor to the Lana-Liss combination used in GA7.1.

The use of Liss and Merlivat (1986) is supported by recent direct measurements of DMS air-sea exchange, which reported lower gas transfer velocities across the air-sea interface for DMS (Yang et al., 2011) than previous works which were largely based on CO_2 measurements (Wanninkhof, 1992). The higher solubility of DMS is likely the leading cause for the different transfer velocities, particularly at high wind speeds (Bell et al., 2013; Wanninkhof, 2014).

The results from Figures 10 and 11 are consistent with the stronger seasonal cycle of CDNC observed on GA6.0. Other things being equal, this could explain the differences in cloud droplet size between the two model configurations. However, Figure 12 shows that the seasonal cycle of atmospheric concentration of DMS in a layer centered at 800 m high is stronger in GA7.1, both in the control and in the climate change response. This suggests that the sinks of atmospheric DMS operate in very different ways in CLASSIC and GLOMAP: DMS in CLASSIC is more readily oxidized to sulfur dioxide and subsequently sulfate aerosol because of differences in the DMS chemistry and the use of different oxidant fields to drive this chemistry.

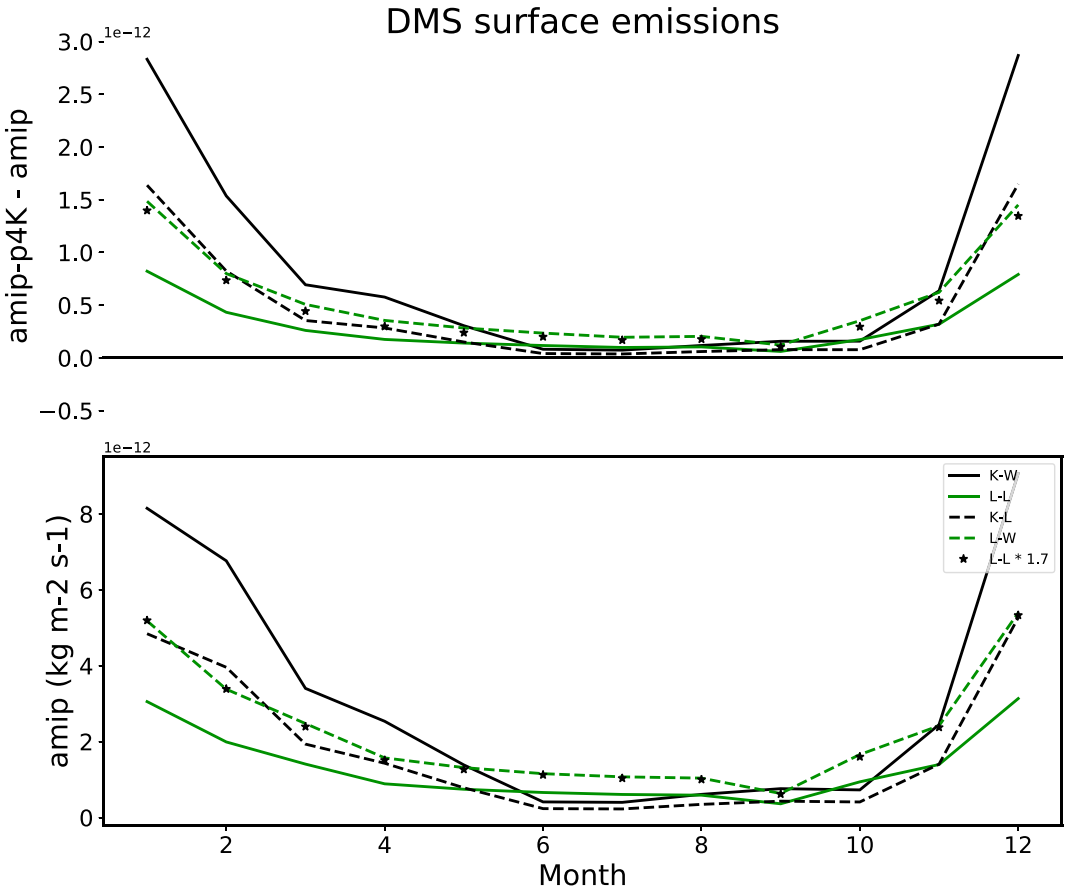

Figure 11. Seasonal cycle of dimethyl sulfide (DMS) surface emissions using different combinations of seawater concentration and emission parametrizations: Kettle-Wanninkhof (K-W), Lana-Liss (L-L), Kettle-Liss (K-L), and Lana-Wanninkhof (L-W). The 1.7 DMS scaling used in GA7.1 is shown by the L-L*1.7 stars. Regional averages between 50°S and 70°S.

It also suggests that, although the DMS concentration in seawater and emission parametrizations play a significant role in setting the climatological seasonal cycle of atmospheric DMS concentrations, they are not the main drivers of the differences in the cloud droplet effective radius response under climate change.

The main control of the difference in cloud droplet effective radius climate change response between GA6.0 and GA7.1 can be explained by the different sensitivities of CDNC to changes in DMS atmospheric concentration. Figure 13 shows CDNC-DMS joint probability distributions for the two baseline model configurations for the *amip* and *amip-p4K* experiments. It is clear that CLASSIC is much more sensitive to changes in DMS atmospheric concentration. A large fraction of the time it produces unrealistically small CDNC values of less than 10 cm^{-3} (representing the numerical minimum value set in the code), switching to larger CDNC values when DMS concentration increases above 0.2 nmol/mol. The increase in DMS is driven by the increase in surface wind speed with warming as the jet moves poleward. The increase in surface wind speed is similar across all seasons (not shown), but since the climatological winds are weaker in summer, the relative increase is larger in that season, driving the strong seasonal cycle in the CDNC response with warming in GA6.0. Ultimately, this explains the larger increase in CDNC in GA6.0 (Figure 9), in spite of its weaker increase in atmospheric DMS absolute concentration with warming (and only 10% larger in relative terms).

As explained by Bellouin et al. (2013), the different sensitivity is due to the fact that CLASSIC assumes a fixed modal size distribution for sulfate aerosol, and therefore can only respond to changes in DMS emissions by changing the cloud condensation nuclei (CCN) number concentration. However, GLOMAP-mode is able to increase the mean size of its soluble modes via condensation of sulfuric acid. The GLOMAP-mode response

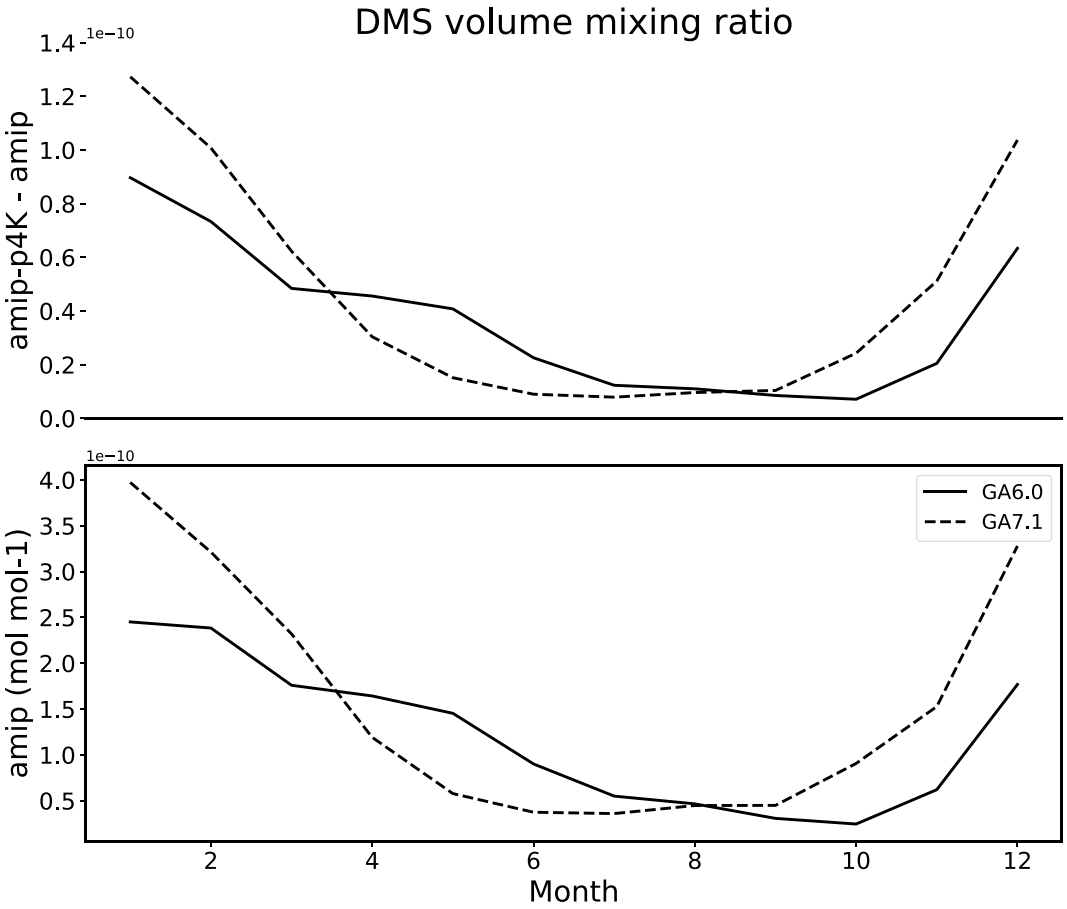

Figure 12. Seasonal cycle of dimethyl sulfide (DMS) atmospheric concentration in a layer centered at 800 m above the surface. Regional averages between 50°S and 70°S.

should be more realistic because aqueous-phase oxidation of DMS-derived sulfur dioxide (SO_2) does not create new CCN, it only grows existing CCN (Woodhouse et al., 2013).

The fairly insensitive relation between DMS concentration and CDNC in GA7.1 explains the nearly null (albeit slightly positive) response of CDNC with warming (Figure 9). For a constant LWP, the small increase in CDNC would decrease the cloud droplet size. Given that the cloud droplet size increases slightly with warming in GA7.1, we conclude that the increase in CDNC must be compensated by the increase in LWP (Figure 6f), which will tend to increase the droplet size. Using the fact that the cloud droplet effective radius in GA7.1 is proportional to $(LWC/CDNC)^{-0.19}$, we can estimate the fractional change in effective radius as approximately $0.2(\Delta LWP/LWP - \Delta CDNC/CDNC)$. Using the values for January in Figures 6d and 9, we estimate an increase in droplet radius of about 0.6 μm. This is larger than the actual increase of around 0.3 μm but confirms that the LWP changes drive a cloud droplet size increase of the same order than the one observed in GA7.1.

7. Discussion

The model changes introduced between GC2.0 and GC3.1 have significantly reduced the magnitude of the feedback parameter. Within this context, it is worth looking at the model feedbacks in absolute terms, not only relative to previous model configurations. It is interesting to notice that many models seem to show a shortwave feedback dipole in the Southern Ocean, with a negative feedback in the high midlatitudes, and positive in the low midlatitudes (Ceppi et al., 2016). The latitude at which the feedback switches from positive to negative ranges between 40°S and 55°S. GA6.0 is a canonical example of this behavior, with a transition from positive to negative feedback at 50°S, approximately (Figure 5b). Recent studies have shown that interannual variability metrics can be used as proxies for long-term climate feedbacks (Ceppi et al., 2016;

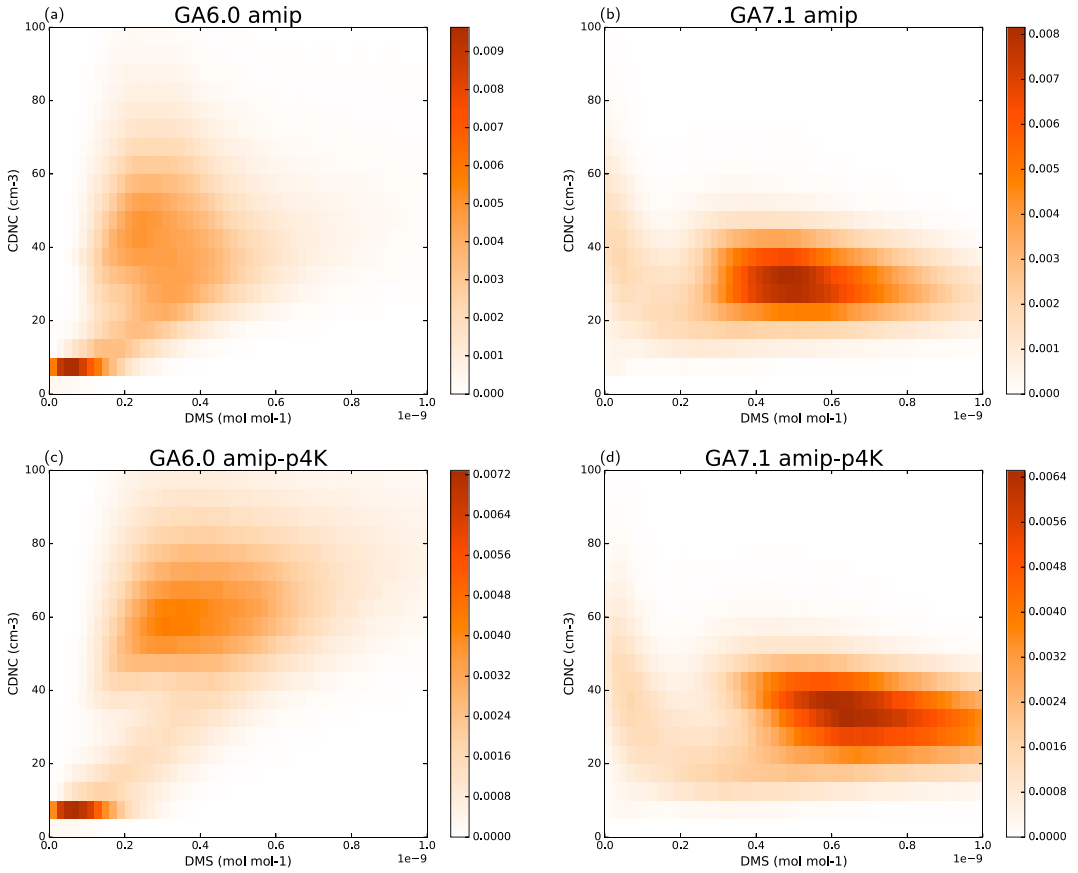

Figure 13. Joint frequency histogram of cloud droplet number concentration (CDNC) and dimethyl sulfide (DMS) atmospheric concentration in a layer centered at 800 m above the surface. Data for region between 50°S and 70°S.

Gordon & Klein, 2014; Terai et al., 2016). The study by Ceppi et al. (2016) does not support the existence of this dipole in the shortwave feedback. It shows a negative SW feedback across the entire region, with values up to -2 W·m^{-2}·K^{-1}, although typically not below -1 W·m^{-2}·K^{-1}, depending on the observational data set used in the analysis. Models tend to show a stronger negative SW feedback in the Southern Hemisphere high midlatitudes. Terai et al. (2016) shows a larger discrepancy between models and observations, with models having a too strong optical depth feedback in those regions. Although more work is needed to understand the differences and uncertainties in observational estimates, this suggests that the negative lobe in GA6.0 and GA7.1 is probably consistent with the observed estimates, with GA7.1 being perhaps closer to the observed estimates. However, the positive lobe in both models is not consistent with the observational proxies (less so in GA7.1), in common with many other models (Ceppi et al., 2016; McCoy et al., 2014). This poses the interesting question of whether the strongly positive cloud fraction feedback that both GA6.0 and GA7.1 show in the region between 30°S and 50°S is realistic at all. It also suggests the possibility that this strong cloud fraction feedback was partially muted by two overly strong negative feedbacks in GA6.0: aerosol-cloud interaction and cloud phase-change feedback. Some studies indeed suggest that models have a too strong aerosol-cloud interaction (Chen et al., 2012; Sato et al., 2018; Stevens, 2015), although there is no consensus yet on this topic (Malavelle et al., 2017; Rosenfeld et al., 2019).

McCoy et al. (2016) shows that the CMIP5 ensemble shows a negative correlation between the present-day cloud fraction and LWP for the midlatitudes, that is, models with more LWP have less cloud fraction. They attribute this correlation to tuning of the climate mean state cloud fraction to compensate for midlatitude cloud albedo changes produced by mixed-phase parameterizations. Our results do not seem to follow this correlation, since GA7.1 shows both an increase in liquid cloud fraction (Figure 8) and in LWP (Figure 6d) with respect to GA6.0. Whether this is a product of a more realistic representation of mixed-phase cloud processes in GA7.1 or a result of tuning is difficult to say.

Although these arguments are admittedly speculative, we think that any top-down tuning of a model's global-mean feedback (or ECS) to independent estimates may not necessarily improve the fidelity of the simulations. In other words, the fact that a model has an ECS within the range provided by independent estimates (e.g., Stevens et al., 2016) does not imply that the model is representing all the feedbacks correctly. From the model-development perspective, our efforts as a community should focus on improving understanding of the underlying processes and finding observational process-based metrics that are capable of constraining the processes that control the models' radiative feedbacks, expanding on the recent work on feedback proxies, both in the midlatitudes (e.g., Ceppi et al., 2016; Gordon & Klein, 2014), and in the tropics (e.g., McCoy et al., 2018; Myers & Norris, 2015; Qu et al., 2015). Of course, the assumption here is that the relationship between these processes and the long-term feedbacks holds in the real world. Our arguments are very similar in spirit to those made by other studies that focused on contrasting emergent constraints on climate sensitivity with those for individual feedback mechanisms (Caldwell et al., 2011; Hall et al., 2019; Klein & Hall, 2015).

8. Conclusions

We analyze the model changes that control most of the increase in the feedback parameter between the latest two configurations of the Hadley Centre climate model, GC2.0 and GC3.1. We follow an experimental protocol similar to Gettelman et al. (2012), and use atmosphere-only simulations to track down the main processes that drive the changes in feedbacks. We run a large suite of experiments that test the effect of individual developments that were implemented between GA6.0 and GA7.1, the atmospheric components of GC2.0 and GC3.1, respectively.

These experiments show that two developments are the leading contributors to the differences in feedbacks: the replacement of the CLASSIC aerosol scheme by the GLOMAP-mode scheme, and the introduction of a new mixed-phase cloud parameterization. Both schemes contribute to increasing the shortwave cloud feedback in the midlatitudes, either by reducing the strength of the existing negative feedback in the high midlatitudes (50–70°S), or by enhancing the existing positive feedback in the lower midlatitudes (30–50°S). We show that, although both the new aerosol and mixed-phase schemes change the shortwave feedback in the same direction, they operate through fundamentally different mechanisms.

The mixed-phase scheme increases the climatological cloud LWP and reduces its increase with warming, with both effects contributing to the increase in the feedback parameter. The increase of LWP in the present-day reduces the radiative efficiency of the LWP increase with warming. The weakening of the response is consistent with the expected behavior of reduced influence of a phase-change negative radiative feedback with more supercooled liquid water in the present-day climate, more in line with the observations. The increase in LWP makes the model's climatology close to the microwave satellite retrievals, and the liquid cloud fraction is also better represented in the new model. This scheme also enhances a positive cloud fraction radiative feedback that is potentially unrealistic.

The new aerosol scheme, GLOMAP-mode, suppresses a strong negative feedback that operates through a reduction in cloud droplet size, which increases the cloud albedo with warming. GLOMAP-mode shows a much less sensitive relationship between the CDNC and changes in the concentration of DMS. Since sulfate aerosol produced from DMS is one of the main contributors to CDNC in the Southern Ocean, the change in the DMS-CDNC relationship suppresses the large cloud effective radius decrease with warming. A less sensitive DMS-CDNC relationship is considered a more realistic representation of the aerosol processes, allowing the aerosol mass to grow without increasing the number concentration (Woodhouse et al., 2013). GLOMAP-mode also has a significant impact on the cloud climatology, reducing the climatological effective radius. This compares worse with the satellite retrievals, which report droplet sizes larger than those in GA6.0, although the retrievals are potentially subject to large positive biases. At the same time, the CDNC increases in GA7.1 taking it closer to the observational estimates, although both models still underestimate CDNC. The cloud droplet size and CDNC comparisons are difficult to reconcile, because they would imply a massive model underestimate in LWP, which is not supported by independent comparisons against microwave retrievals. This is probably pointing to the fact that the droplet size and CDNC satellite retrievals are subject to large errors in these latitudes. Further work in validating and improving the satellite retrievals should be a priority if we want to better constrain microphysical cloud properties in models.

Both the LWP and cloud droplet size climatological changes make the control clouds brighter, which are now probably too bright in the region between 30°S and 50°S (Williams & Bodas-Salcedo, 2017; Williams et al., 2018). This has implications for the cloud feedback, as it enhances the strength of the strong positive cloud fraction shortwave feedback that GA6.0 shows in this region. It is therefore clear that the background climatology of cloud properties also plays an important role in modulating the strength of the cloud feedbacks.

Acknowledgments
This work was supported by the Met Office Hadley Centre Climate Programme funded by BEIS and Defra. Elsaesser was funded via a subcontract with the Jet Propulsion Laboratory (JPL) (Grant GG008658) to create the MAC-LWP product, an enhanced climate data record (CDR) funded through the NASA Making Earth System Data Records for Use in Research Environments (MEaSUREs) Program under RTOP WBS 105324/547714.04.14.01.54. We thank F. Malavelle and D. Grosvenor for providing us with the MODIS C6.1 cloud effective radius retrievals and CDNC data, respectively. We thank C. Senior, M. Webb, and D. Sexton for their comments. The simulation data used in this study are archived at the Met Office and are available for research purposes through the JASMIN platform (www.jasmin.ac.uk) maintained by the Centre for Environmental Data Analysis (CEDA); for details please contact UM_collaboration@metoffice.gov.uk referencing this paper. CERES data were obtained from the NASA Langley Research Center Atmospheric Science Data Center. MAC LWP data can be obtained from the NASA GES DISC Data Archive (disc.gsfc.nasa.gov). MODIS C5.1 cloud particle size and CALIPSO-GOCCP data were obtained from the IPSL ClimServ data centre (climserv.ipsl.polytechnique.fr/cfmip-obs.html). We thank two anonymous reviewers that improved the quality of the manuscript with their constructive comments.

References

Andrews, T., Gregory, J. M., Webb, M. J., & Taylor, K. E. (2012). Forcing, feedbacks and climate sensitivity in CMIP5 coupled atmosphere-ocean climate models. *Geophysical Research Letters*, *39*, L09712. https://doi.org/10.1029/2012GL051607

Bell, T. G., De Bruyn, W., Miller, S. D., Ward, B., Christensen, K. H., & Saltzman, E. S. (2013). Air-sea dimethylsulfide (DMS) gas transfer in the north atlantic: evidence for limited interfacial gas exchange at high wind speed. *Atmospheric Chemistry and Physics*, *13*(21), 11,073–11,087. https://doi.org/10.5194/acp-13-11073-2013

Bellouin, N., Mann, G. W., Woodhouse, M. T., Johnson, C., Carslaw, K. S., & Dalvi, M. (2013). Impact of the modal aerosol scheme GLOMAP-mode on aerosol forcing in the Hadley Centre global environmental model. *Atmospheric Chemistry and Physics*, *13*, 3027–3044. https://doi.org/10.5194/acp-13-3027-2013

Bellouin, N., Rae, J., Jones, A., Johnson, C., Haywood, J., & Boucher, O. (2011). Aerosol forcing in the climate model intercomparison project (CMIP5) simulations by hadGEM2-ES and the role of ammonium nitrate. *Journal of Geophysical Research*, *116*, D20206. https://doi.org/10.1029/2011jd016074

Bennartz, R., & Rausch, J. (2017). Global and regional estimates of warm cloud droplet number concentration based on 13 years of AQUA-MODIS observations. *Atmospheric Chemistry and Physics*, *17*, 9815–9836. https://doi.org/10.5194/acp-17-9815-2017

Bodas-Salcedo, A. (2018). Cloud condensate and radiative feedbacks at midlatitudes in an aquaplanet. *Geophysical Research Letters*, *45*, 3635–3643. https://doi.org/10.1002/2018GL077217

Bodas-Salcedo, A., Andrews, T., Karmalkar, A. V., & Ringer, M. A. (2016b). Cloud liquid water path and radiative feedbacks over the Southern Ocean. *Geophysical Research Letters*, *43*, 10,938–10,946. https://doi.org/10.1002/2016GL070770

Bodas-Salcedo, A., Hill, P. G., Furtado, K., Williams, K. D., Field, P. R., Manners, J. C., et al. (2016a). Large contribution of supercooled liquid clouds to the solar radiation budget of the Southern Ocean. *Journal of Climate*, *29*(11), 4213–4228. https://doi.org/10.1175/JCLI-D-15-0564.1

Bodas-Salcedo, A., Webb, M. J., Bony, S., Chepfer, H., Dufresne, J. L., Klein, S., et al. (2011). COSP: Satellite simulation software for model assessment. *Bulletin of the American Meteorological Society*, *92*(8), 1023–1043. https://doi.org/10.1175/2011BAMS2856.1

Bodas-Salcedo, A., Williams, K. D., Ringer, M. A., Beau, I., Cole, J. N. S., Dufresne, J.-L., et al. (2014). Origins of the solar radiation biases over the Southern Ocean in CFMIP2 models. *Journal of Climate*, *27*, 41–56. https://doi.org/10.1175/JCLI-D-13-00169.1

Boers, R., Acarreta, J. R., & Gras, J. L. (2006). Satellite monitoring of the first indirect aerosol effect: Retrieval of the droplet concentration of water clouds. *Journal of Geophysical Research*, *111*, D22208. https://doi.org/10.1029/2005jd006838

Boutle, I. A., & Abel, S. J. (2012). Microphysical controls on the stratocumulus topped boundary-layer structure during VOCALS-REx. *Atmospheric Chemistry and Physics*, *12*, 2849–2863. https://doi.org/10.5194/acp-12-2849-2012

Boutle, I. A., Abel, S. J., Hill, P. G., & Morcrette, C. J. (2014). Spatial variability of liquid cloud and rain: Observations and microphysical effects. *Quarterly Journal of the Royal Meteorological Society*, *140*, 583–594. https://doi.org/10.1002/qj.2140

Caldwell, P. M., Zelinka, M. D., & Klein, S. A. (2011). Evaluating emergent constraints on equilibrium climate sensitivity. *Journal of Climate*, *31*, 3921–3942. https://doi.org/10.1175/JCLI-D-17-0631.1

Ceppi, P., McCoy, D. T., & Hartmann, D. L. (2016). Observational evidence for a negative shortwave cloud feedback in middle to high latitudes. *Geophysical Research Letters*, *43*, 1331–1339. https://doi.org/10.1002/2015GL067499

Cesana, G., & Chepfer, H. (2013). Evaluation of the cloud thermodynamic phase in a climate model using CALIPSO-GOCCP. *Journal of Geophysical Research: Atmospheres*, *118*, 7922–7937. https://doi.org/10.1002/jgrd.50376

Cess, R. D., Potter, G. L., Blanchet, J. P., Boer, G. J., Del Genio, A. D., Déqué, M., et al. (1990). Intercomparison and interpretation of climate feedback processes in 19 atmospheric general circulation models. *Journal of Geophysical Research*, *95*, 16,601–16,615.

Chen, Y.-C., Christensen, M. W., Xue, L., Sorooshian, A., Stephens, G. L., Rasmussen, R. M., & Seinfeld, J. H. (2012). Occurrence of lower cloud albedo in ship tracks. *Atmospheric Chemistry and Physics*, *12*, 8223–8235. https://doi.org/10.5194/acp-12-8223-2012

Chepfer, H., Bony, S., Winker, D., Cesana, G., Dufresne, J.-L., Minnis, P., et al. (2010). The GCM Oriented Calipso Cloud Product (CALIPSO-GOCCP). *Journal of Geophysical Research*, *115*, D00H16. https://doi.org/10.1029/2009JD012251

Chepfer, H., Bony, S., Winker, D., Chiriaco, M., Dufresne, J.-L., & Sèze, G. (2008). Use of CALIPSO lidar observations to evaluate the cloudiness simulated by a climate model. *Geophysical Research Letters*, *35*, L15704. https://doi.org/10.1029/2008GL034207

Doelling, D. R., Loeb, N. G., Keyes, D. F., Nordeen, M. L., Morstad, D., Nguyen, C., et al. (2013). Geostationary enhanced temporal interpolation for ceres flux products. *Journal of Atmospheric and Oceanic Technology*, *30*(6), 1072–1090. https://doi.org/10.1175/JTECH-D-12-00136.1

Elsaesser, G. S., O'Dell, C. W., Lebsock, M. D., Bennartz, R., Greenwald, T. J., & Wentz, F. J. (2017). The multisensor advanced climatology of liquid water path (MAC-LWP). *Journal of Climate*, *30*, 10,193–10,210. https://doi.org/10.1175/JCLI-D-16-0902.1

Eyring, V., Bony, S., Meehl, G. A., Senior, C. A., Stevens, B., Stouffer, R. J., & Taylor, K. E. (2016). Overview of the Coupled Model Intercomparison Project Phase 6 (CMIP6) experimental design and organisation. *Geoscientific Model Development*, *8*, 10,539–10,583. https://doi.org/10.5194/gmdd-8-10539-2015

Furtado, K., Field, P. R., Boutle, I. R., Morcrette, C. J., & Wilkinson, J. M. (2016). A physically-based, subgrid parametrization for the production and maintenance of mixed-phase clouds in a general circulation model. *Journal of the Atmospheric Sciences*, *73*, 279–291. https://doi.org/10.1175/JAS-D-15-0021.1

Gettelman, A., Kay, J. E., & Shell, K. M. (2012). The evolution of climate sensitivity and climate feedbacks in the community atmosphere model. *Journal of Climate*, *25*(2), 1453–1469. https://doi.org/10.1175/JCLI-D-11-00197.1

Gordon, N. D., & Klein, S. A. (2014). Low-cloud optical depth feedback in climate models. *Journal of Geophysical Research: Atmospheres*, *119*, 6052–6065. https://doi.org/10.1002/2013JD021052

Greenwald, T. J., Bennartz, R., Lebsock, M., & Teixeira, J. (2018). An uncertainty data set for passive microwave satellite observations of warm cloud liquid water path. *Journal of Geophysical Research: Atmospheres*, *123*, 3668–3687. https://doi.org/10.1002/2017JD027638

Gregory, J. M., Ingram, W. J., Palmer, M. A., Jones, G. S., Stott, P. A., Thorpe, R. B., et al. (2004). A new method for diagnosing radiative forcing and climate sensitivity. *Geophysical Research Letters*, *31*, L03205. https://doi.org/10.1029/2003gl018747

Grosvenor, D. P., Sourdeval, O., Zuidema, P., Ackerman, A., Alexandrov, M. D., Bennartz, R., et al. (2018). Remote sensing of droplet number concentration in warm clouds: A review of the current state of knowledge and perspectives. *Reviews of Geophysics*, *56*, 409–453. https://doi.org/10.1029/2017RG000593

Grosvenor, D. P., & Wood, R. (2014). The effect of solar zenith angle on MODIS cloud optical and microphysical retrievals within marine liquid water clouds. *Atmospheric Chemistry and Physics*, *14*(), 7291–7321. https://doi.org/10.5194/acp-14-7291-2014

Hall, A., Cox, P., Huntingford, C., & Klein, S. (2019). Progressing emergent constraints on future climate change. *Nature Climate Change*, *9*, 269–278. https://doi.org/10.1038/s41558-019-0436-6

Hamilton, D. S., Lee, L. A., Pringle, K. J., Reddington, C. L., Spracklen, D. V., & Carslaw, K. S. (2014). Occurrence of pristine aerosol environments on a polluted planet. *Proceedings of the National Academy of Sciences*, *111*(52), 18,466–18,471. https://doi.org/10.1073/pnas.1415440111

Hilburn, K. A., & Wentz, F. J. (2008). Intercalibrated passive microwave rain products from the unified microwave ocean retrieval algorithm (UMORA). *Journal of Applied Meteorology and Climatology*, *47*, 778–794. https://doi.org/10.1175/JCLI-D-17-0586.1

Hill, P. G., Manners, J., & Petch, J. C. (2011). Reducing noise associated with the monte carlo independent column approximation for weather forecasting models. *Quarterly Journal of the Royal Meteorological Society*, *137*, 219–228. https://doi.org/10.1002/qj.732

Hyder, P., Edwards, J. M., Allan, R. P., Hewitt, H. T., Bracegirdle, T. J., Gregory, J. M., et al. (2018). *Critical Southern Ocean climate model biases traced to atmospheric model cloud errors*, vol. 9, pp. 4105. https://doi.org/10.1038/s41467-018-05634-2

Kettle, A. J., Andreae, M. O., Amouroux, D., Andreae, T. W., Bates, T. S., Berresheim, H., et al. (1999). A global database of sea surface dimethylsulfide (DMS) measurements and a procedure to predict sea surface dms as a function of latitude, longitude, and month. *Global Biogeochemical Cycles*, *13*, 399–444.

King, M. D., Menzel, W. P., Kaufman, Y. J., Tanre, D., Gao, B. C., Platnick, S., et al. (2003). Cloud and aerosol properties, precipitable water, and profiles of temperature and humidity from MODIS. *IEEE Transactions on Geoscience and Remote Sensing*, *41*, 442–458. https://doi.org/10.1109/TGRS.2002.808226

Klein, S. A., & Hall, A. (2015). Emergent constraints for cloud feedbacks. *Current Climate Change Reports*, *1*, 276–287. https://doi.org/10.1007/s40641-015-0024-4

Klein, S. A., & Jakob, C. (1999). Validation and sensitivities of frontal clouds simulated by the ECMWF model. *Monthly Weather Review*, *127*(10), 2514–2531.

Lana, A., Bell, T. G., Simó, R., Vallina, S. M., Ballabrera-Poy, J., Kettle, A. J., et al. (2011). An updated climatology of surface dimethlysulfide concentrations and emission fluxes in the global ocean. *Global Biogeochemical Cycles*, *25*, GB1004. https://doi.org/10.1029/2010GB003850

Lebsock, M., & Su, H. (2014). Application of active spaceborne remote sensing for understanding biases between passive cloud water path retrievals. *Journal of Geophysical Research: Atmospheres*, *119*, 8962–8979. https://doi.org/10.1002/2014JD021568

Liang, L., Girolamo, L. D., & Sun, W. (2015). Bias in MODIS cloud drop effective radius for oceanic water clouds as deduced from optical thickness variability across scattering angles. *Journal of Geophysical Research: Atmospheres*, *120*, 7661–7681. https://doi.org/10.1002/2015JD023256

Liss, P. S., & Merlivat, L. (1986). Air-sea gas exchange rates: Introduction and synthesis. In P. BuatMenard (Ed.), *The role of air-sea exchange in geochemical cycling* pp. 113–127). Dordrecht: Reidel.

Liu, Y., Daum, P. H., Guo, H., & Peng, Y. (2008). Dispersion bias, dispersion effect, and the aerosol-cloud conundrum. *Environmental Research Letters*, *3*, 045021. https://doi.org/10.1088/1748-9326/3/4/045021

Lohmann, U., & Neubauer, D. (2018). The importance of mixed-phase and ice clouds for climate sensitivity in the global aerosol-climate model ECHAM6-HAM2. *Atmospheric Chemistry and Physics*, *18*, 8807–8828. https://doi.org/10.5194/acp-18-8807-2018

Malavelle, F. F., Haywood, J. M., Jones, A., Gettelman, A., & authors, co (2017). Strong constraints on aerosol-cloud interactions from volcanic eruptions. *Nature*, *546*, 485–491. https://doi.org/10.1038/nature22974

Mann, G. W., Carslaw, K. S., Ridley, D. A., Spracklen, D. V., Pringle, K. J., Merikanto, J., et al. (2012). Intercomparison of modal and sectional aerosol microphysics representations within the same 3-D global chemical transport model. *Atmospheric Chemistry and Physics*, *12*(10), 4449–4476. https://doi.org/10.5194/acp-12-4449-2012

Mann, G. W., Carslaw, K. S., Spracklen, D. V., Ridley, D. A., Manktelow, P. T., Chipperfield, M. P., et al. (2010). Description and evaluation of GLOMAP-MODE: A modal global aerosol microphysics model for the UKCA composition-climate model. *Geoscientific Model Development*, *3*, 519–551. https://doi.org/10.5194/gmd-3-519-2010

McCoy, D. T., Field, P. R., Schmidt, A., Grosvenor, D. P., Bender, F. A.-M., Shipway, B. J., et al. (2018). The aerosol-cyclone indirect effect in observations and high-resolution simulations. *Atmospheric Chemistry and Physics*, *18*(8), 5821–5846. https://doi.org/10.5194/acp-18-5821-2018

McCoy, D. T., Hartmann, D. L., & Grosvenor, D. P. (2014). Observed southern ocean cloud properties and shortwave reflection. Part II: Phase changes and low cloud feedback. *Journal of Climate*, *27*, 8858–8868. https://doi.org/10.1175/JCLI-D-14-00288.1

McCoy, D. T., Tan, I., Hartmann, D. L., Zelinka, M. D., & Storelvmo, T. (2016). On the relationships among cloud cover, mixed-phase partitioning, and planetary albedo in GCMs. *Journal of Advances in Modeling Earth Systems*, *8*, 650–668. https://doi.org/10.1002/2015MS000589

Mulcahy, J. P., Jones, C., Sellar, A., Johnson, B., Boutle, I. A., Jones, A., et al. (2018). Improved aerosol processes and effective radiative forcing in HadGEM3 and UKESM1. *Journal of Advances in Modeling Earth Systems*, *10*, 2786–2805. https://doi.org/10.1029/2018MS001464

Myers, T. A., & Norris, J. R. (2015). On the relationships between subtropical clouds in meteorology in observations and CMIP3 and CMIP5 models. *Journal of Climate*, *28*, 2945–2967. https://doi.org/10.1175/JCLI-D-14-00475.1

O'Dell, C. W., Wentz, F. J., & Bennartz, R. (2008). Cloud liquid water path from satellite-based passive microwave observations: a new climatology over the global oceans. *Journal of Climate*, *21*, 1721–1739. https://doi.org/10.1175/2007JCLI1958.1

Pincus, R., Barker, H. W., & Morcrette, J.-J. (2003). A fast, flexible, approximate technique for computing radiative transfer in inhomogeneous cloud fields. *Journal of Geophysical Research*, *108*(D13), 4376. https://doi.org/10.1029/2002JD003322

Pincus, R., Platnick, S., Ackerman, S. A., Hemler, R. S., & Hofmann, R. J. P. (2012). Reconciling simulated and observed views of clouds: MODIS, ISCCP, and the limits of instrument simulators. *Journal of Climate*, *25*(13), 4699–4720. https://doi.org/10.1175/JCLI-D-11-00267.1

Platnick, S., Ackerman, S. A., King, M. D., Meyer, K., Menzel, W. P., Holz, R. E., et al. (2015). *MODIS atmosphere L2 cloud product (06_L2), NASA MODIS Adaptive Processing System*. USA: Goddard Space Flight Center. https://doi.org/10.5067/MODIS/MOD06_L2.006

Platnick, S., Meyer, K. G., King, M. D., Wind, G., Amarasinghe, N., Marchant, B., et al. (2017). The MODIS cloud optical and microphysical products: Collection 6 updates and examples from terra and aqua. *IEEE Transactions on Geoscience and Remote Sensing*, *55*, 502–525. https://doi.org/10.1109/tgrs.2016.2610522

Qu, X., Hall, A., Klein, S. A., & DeAngelis, A. M. (2015). Positive tropical marine low-cloud cover feedback inferred from cloud-controlling factors. *Geophysical Research Letters*, *42*, 7767–7775. https://doi.org/10.1002/2015GL065627

Ringer, M. A., Andrews, T., & Webb, M. J. (2014). Global-mean radiative feedbacks and forcing in atmosphere-only and coupled atmosphere-ocean climate change experiments. *Geophysical Research Letters*, *41*, 4035–4042. https://doi.org/10.1002/2014GL060347

Rosenfeld, D., Zhu, Y., Wang, M., Zheng, Y., Goren, T., & Yu, S. (2019). Aerosol-driven droplet concentrations dominate coverage and water of oceanic low-level clouds. *Science*, 363. https://doi.org/10.1126/science.aav0566

Rossow, W. B., & Schiffer, R. A. (1999). Advances in understanding clouds from ISCCP. *Bulletin of the American Meteorological Society*, *80*, 2261–2287.

Sato, Y., Goto, D., Michibata, T., Suzuki, K., Takemura, T., Tomita, H., & Nakajima, T. (2018). Aerosol effects on cloud water amounts were successfully simulated by a global cloud-system resolving model. *Nature Communications*, *9*(1), 985. https://doi.org/10.1038/s41467-018-03379-6

Senior, C. A., Andrews, T., Burton, C., Chadwick, R., Copsey, D., Graham, T., et al. (2016). Idealized climate change simulations with a high-resolution physical model: Hadgem3-gc2. *Journal of Advances in Modeling Earth Systems*, *8*, 813–830. https://doi.org/10.1002/2015MS000614

Stephens, G. L. (1978). Radiation profiles in extended water clouds. II: Parameterization schemes. *Journal of the Atmospheric Sciences*, *35*, 2123–2132. https://doi.org/10.1175/1520-0469(1978)035<2123:RPIEWC>2.0.CO;2

Stevens, B. (2015). Rethinking the lower bound on aerosol radiative forcing. *Journal of Climate*, *28*(), 4794–4819. https://doi.org/10.1175/JCLI-D-14-00656.1

Stevens, B., Sherwood, S. C., Bony, S., & Webb, M. J. (2016). Prospects for narrowing bounds on Earth's equilibrium climate sensitivity. *Earth's Future*, *4*, 512–522. https://doi.org/10.1002/2016EF000376

Tan, I., Storelvmo, T., & Zelinka, M. D. (2016). Observational constraints on mixed-phase clouds imply higher climate sensitivity. *Science*, *352*, 224–227. https://doi.org/10.1126/science.aad5300

Taylor, K. E., Crucifix, M., Braconnot, P., Hewitt, C. D., Doutriaux, C., Broccoli, A. J., et al. (2007). Estimating shortwave radiative forcing and response in climate models. *Journal of Climate*, *20*, 2530–2543.

Terai, C. R., Klein, S. A., & Zelinka, M. D. (2016). Constraining the low-cloud optical depth feedback at middle and high latitudes using satellite observations. *Journal of Geophysical Research: Atmospheres*, *121*, 9696–9716. https://doi.org/10.1002/2016JD025233

Walters, D., Baran, A., Boutle, I., Brooks, M., Earnshaw, P., Edwards, J., et al. (2019). The met offce unifed model global atmosphere 7.0/7.1 and JULES global land 7.0 configurations. *Geoscientific Model Development*, *12*, 1909–1963. https://doi.org/10.5194/gmd-12-1909-2019

Walters, D., Boutle, I., Brooks, M., Melvin, T., Stratton, R., Vosper, S., et al. (2017). The met office unified model global atmosphere 6.0/6.1 and JULES global land 6.0/6.1 configurations. *Geoscientific Model Development*, *10*, 1487–1520. https://doi.org/10.5194/gmd-10-1487-2017

Wanninkhof, R. (1992). Relationship between wind speed and gas exchange over the ocean. *Journal of Geophysical Research*, *97*, 7373–7382.

Wanninkhof, R. (2014). Relationship between wind speed and gas exchange over the ocean revisited. *Limnology and Oceanography: Methods*, *12*(6), 351–362. https://doi.org/10.4319/lom.2014.12.351

Webb, M. J., Andrews, T., Bodas-Salcedo, A., Bony, S., Bretherton, C. S., Chadwick, R., et al. (2017). The Cloud Feedback Model Intercomparison Project (CFMIP) contribution to CMIP6. *Geoscientific Model Development*, *10*, 359–384. https://doi.org/10.5194/gmd-10-359-2017

Webb, M., Senior, C., Bony, S., & Morcrette, J. J. (2001). Combining ERBE and ISCCP data to assess clouds in the Hadley Centre, ECMWF and LMD atmospheric climate models. *Climate Dynamics*, *17*, 905–922.

West, R. E. L., Stier, P., Jones, A., Johnson, C. E., Mann, G. W., Bellouin, N., et al. (2014). The importance of vertical velocity variability for estimates of the indirect aerosol effects. *Atmospheric Chemistry and Physics*, *14*(12), 6369–6393. https://doi.org/10.5194/acp-14-6369-2014

Williams, K. D., & Bodas-Salcedo, A. (2017). A multi-diagnostic approach to cloud evaluation. *Geoscientific Model Development*, *10*, 2547–2566. https://doi.org/10.5194/gmd-10-2547-2017

Williams, K. D., Copsey, D., Blockley, E. W., Bodas-Salcedo, A., Calvert, D., Comer, R., et al. (2018). The Met Office global coupled model 3.0 and 3.1 (GC3.0 and GC3.1) configurations. *Journal of Advances in Modeling Earth Systems*, *10*, 357–380. https://doi.org/10.1002/2017MS001115

Williams, K. D., Harris, C. M., Bodas-Salcedo, A., Camp, J., Comer, R. E., Copsey, D., et al. (2015). The Met Office global coupled model 2.0 (GC2) configuration. *Geoscientific Model Development*, *8*, 1509–1524. https://doi.org/10.5194/gmd-8-1509-2015

Woodhouse, M. T., Mann, G. W., Carslaw, K. S., & Boucher, O. (2013). Sensitivity of cloud condensation nuclei to regional changes in dimethyl-sulphide emissions. *Atmospheric Chemistry and Physics*, *13*, 2723–2733. https://doi.org/10.5194/acp-13-2723-2013

Yang, M., Blomquist, B. W., Fairall, C. W., Archer, S. D., & Huebert, B. J. (2011). Air-sea exchange of dimethylsulfide in the southern ocean: Measurements from SO GasEx compared to temperate and tropical regions. *Journal of Geophysical Research*, *116*, C00F05. https://doi.org/10.1029/2010JC006526